NASA CR 135175

AN ANALYTICAL METHOD FOR PREDICTING THE AERODYNAMIC PERFORMANCE OF A TURBINE CASCADE WITH FILM COOLING

by

E. McFarland and W. Tabakoff

Supported by:

NATIONAL AERONAUTICS AND SPACE ADMINISTRATION

Lewis Research Center

Contract NGR 36-004-064

1. Report No.	2. Government Accession No.	3. Recipient's Catalog No.
NASA CR 135175		

4. Title and Subtitle	5. Report Date
AN ANALYTICAL METHOD FOR PREDICTING THE AERODYNAMIC PERFORMANCE OF A TURBINE CASCADE WITH FILM COOLING	March 1977
	6. Performing Organization Code

7. Author(s)	8. Performing Organization Report No.
E. McFarland and W. Tabakoff	
	10. Work Unit No.

9. Performing Organization Name and Address	11. Contract or Grant No.
Department of Aerospace Engineering & Applied Mechanics University of Cincinnati Cincinnati, Ohio 45221	NASA NGR 36-004-064
	13. Type of Report and Period Covered
12. Sponsoring Agency Name and Address	Contractor Report
National Aeronautical and Space Administration Washington, D.C. 20546	14. Sponsoring Agency Code

15. Supplementary Notes

16. Abstract

An analytical study was made of the aerodynamic performance of film cooled turbine blades. Various analytical approaches to predicting the performance of film cooled turbine blades are reviewed. A two-dimensional cascade flow solution is developed for calculating the effects of the coolant injection on the total flow field. This solution is used with an available analytical performance predicting method to provide an improved method. Comparisons are made with experimental data and other analytical results.

17. Key Words (Suggested by Author(s))	18. Distribution Statement
Turbine Stator blade Aerodynamics Film cooling Cascade flow	Unclassified - unlimited STAR Category 02

19. Security Classif. (of this report)	20. Security Classif. (of this page)	21. No. of Pages	22. Price*
Unclassified	Unclassified	96	

* For sale by the National Technical Information Service, Springfield, Virginia 22161

TABLE OF CONTENTS

SUMMARY

An investigation was made of various available analytical methods for predicting the aerodynamic performance of film cooled turbine blades. The methods were cataloged according to their basic approaches to the film cooling problem. Each method is briefly described, and an attempt is made to improve upon one of the methods.

The improvements to the method involved the development of a technique to calculate cascade body surface pressure distributions with the effects of coolant injection on these distributions included. This is accomplished by using an integral equation solution for the potential cascade flow. The solution involves using a minimization criteria on the singularity density distributions which in turn are used to calculate the potential flow. The minimization technique was originally developed for the isolated airfoil problem and is extended in this report to cascades. Comparisons of calculated cascade blade surface pressure distributions with other analytical solutions and experimental data are made, and good agreement is shown.

The modified method, which includes the coolant and primary flow interaction effects, was used to predict the aerodynamic performance of a film cooled turbine cascade for which cold flow experimental data was available. The method is in good agreement with experimental results, but offers little improvement over the performance predictions of previous methods. However some insight is gained as to the effects of the coolant injection on the total flow field such as interactions with primary flow, interactions between coolant rows, injection induced separations, coolant mass flow distribution in full film cooling, and the onset of sonic injection conditions.

Finally the method is used to make an analysis of a possible film cooling configuration. This analysis demonstrates the capabilities of the method for use in the design of film cooled turbine blades.

INTRODUCTION

Background

With the increased use of turbofan and turboprop engines, a need has developed for higher turbine inlet temperatures. These higher turbine temperatures produce higher energy levels in the overall thermodynamic cycle so that more efficient engine designs can be made. This additional energy is also required to power the fan and prop components of these engines. Film cooling is one of the better methods of increasing turbine inlet temperatures. The film cooling process consists of injecting a coolant into the mainstream so that it forms a layer of cool fluid which protects the turbine components from the hot combustion gases. Although injection or film cooling is known to be an effective means of allowing increases in turbine inlet temperatures, little is known about the effect it has on turbine aerodynamic performance, and even less about the local fluid dynamics of the injection process. In the present work, an analytical method is developed to predict these performance effects and to model the local inviscid fluid dynamic of the coolant injection process. The analysis is then used to study the effects of film cooling on turbine aerodynamics.

The complexity of the actual turbine film cooling problem prevents one from solving it directly. The combination of three dimensional, unsteady and rotational fluid flow effects plus the heat transfer between the cooling fluid and blade surfaces cannot be included in a single solution. In order to produce a manageable model of film cooling, several simplifying assumptions must be made. The present study deals with steady inviscid irrotational adiabatic flow through a two-dimensional cascade with injection. The solution also includes the effects of compressibility, viscous losses, and the flow characteristics of the coolant ports. Figure 1 shows the basic parameters of the problem. The analysis is developed for known inlet and internal blade flow conditions. The downstream flow conditions and injection velocities are determined during the course of the solution.

Literature Review

Before analyzing the aerodynamic performance of film cooled turbine cascades, one has to gain an appreciation of the various basic techniques for the aerodynamic evaluation of turbomachinery blades. References [1] and [2] are two general works that treat the aerodynamic design of turbomachines. Stewart's [3] method is the classic analysis used by most designers in evaluating the performance of cascades. This method can be used in a totally analytical study as it was originally intended, or to reduce experimental data as described by Prust [4].

The number of film cooling studies was limited before the late 1960's. References [5] through [8] represent a cross-section of the work presented during that time. Also text books such as Schlichting [9] and Kays [10] have sections on the general problem of fluid injection into a main stream. From the late 1960's to the present, a considerable amount of research has been conducted on the film cooling process. Much of this research was instigated by the need for high temperature turbine components. References [11] and [12] give comprehensive information on the turbine cooling problem.

Few studies concentrated on the aerodynamic losses associated with injection processes. References [13] through [16] represent reports from NASA Lewis Research Center's on-going experimental program. Hartzel [17] and Hiroki and Katsumata [18] investigated experimentally turbine cascade aerodynamic losses as well as heat transfer characteristics. An experimental study of an actual turbine is presented by Lokai and Kumirou [19], but the predominant coolant discharge was radially out of the blades end plate and from the blades trailing edge. In the analytical studies of Prust [20] and Hartzel [21] mass averaging mixing theories were used to resolve the film cooled cascade performance problem. Tabakoff and Hamed [22] approached the problem using boundary layer concepts.

A number of analytical studies investigated the effect of injection on the boundary layer of the primary flow. While references [23] through [28] were concerned with the laminar boundary layer problem, Herring [29] analyzed turbulent boundary

layers with injection. Experimental data to complement Herring's analysis can be found in reference [30]. Most of the boundary layer studies listed above included comments on heat transfer. Goldstein [31] and Ekert [32] describe some of the analytical aspects of the heat transfer problem. Experimental work on the same subject can be found in references [33] through [41].

Since potential flow integral equation solutions are used in the analysis of this report, some of the available studies in the field will be discussed. A review of the various techniques for solving the integral equation problem is given by Hess [42]. Two methods of solution have evolved. One uses a vortex singularity distribution as described by Martensen [43], and the other uses a combination of vortex and source-sink singularity distributions [44]. In this study the second method is employed, but examples of the use of Martensen method can be found in references [45] and [46]. The source-sink and vortex combination method has been continually developed and refined. Hess [47] described a method for obtaining higher order solutions. Geising [48] and Geising and Smith [49] extended the method to cascades and hydrofoils. Bristow [50] presented a singularity density minimization technique which produced a higher accuracy first order method. A rapid solution method was demonstrated by Dilley [51] for possible use in interacting boundary layer solutions. A boundary layer corrected potential solution for multi-component airfoils using vortex distributions is reported in reference [52].

The turbine blade shape with its blunt trailing edge poses a question as to how to apply the Kutta condition. Most methods, [42] and [50], simply require that the velocity on the upper and lower surfaces be equal, or that the normal velocity to the trailing edge bisector be zero. Gastelow [53], [54] and Geller [55] offer other possible solutions to the blunt trailing edge problem.

REVIEW OF AVAILABLE ANALYSES

A brief description of the various solution approaches studied is presented. This provides background for the final solution method used in the present work.

Boundary Layer Methods

The boundary layer approach has been used in the past to give loss estimates for cascades without injection. Several solutions have been developed which use a pressure distribution as a driving function for the boundary equations [56], [57]. However, this standard approach fails when applied to the film cooling problem. The Prandtl boundary layer theory assumption that, the dimensionless velocity in the normal direction to the outer flow remain of order $(1/Re)^{1/2}$, is violated by the injection process. Solution of the boundary layer equations with injection has been obtained [24] and [25], when injection velocities were kept very small. Even with the injection velocity maintained at the proper level, the boundary layer can be induced to separate by the injection. The numerical solution usually fails in such cases or produces erratic results. The boundary layer approach has been applied to film cooled cascades with limited success [22]. In this solution, the injection velocities were made small by applying the injection over a larger area than existed in the real case. Furthermore, the solution only produced useful results for injection from the forward portions of the blade where the flow is accelerated causing a favorable pressure gradient. An attempt was made to extend this method by including the inviscid effect of the injection on the outer flow. This inviscid effect was noted experimentally by Bergeles, Gosmann, and Launder [37]. The extension allowed calculation of higher injection velocity flows, but useful solutions were still limited tc the forward regions of the blade.

A study of the available interacting boundary layer techniques for solving the small or closed separation flow problem

points out some of the complexities of the injection process. Such a study could be based on ideas described in references [58] and [59]. In which case, the requirement of a small disturbance due to the injection would limit the study's application in the real film cooling problem. Also, the finite injection area introduces two discontinuities in the flow field at its beginning and end. These discontinuities must be taken into consideration in the problem formulation. Furthermore, if the flow field is subsonic, the effect of the main flow over the port on the injection velocity profile should be considered.

In conclusion, it can be said that present boundary layer methods are not capable of handling the turbine film cooling problem with injection velocities used in actual applications. These methods should prove useful in the transpiration cooled turbine, where the cooling flow is distributed over the entire blade surface. This will keep injection velocities small, eliminate the discontinuities in the boundary conditions, and remove any injection induced separations. The solution will still not be straightforward, since the injection velocity is a function of the pressure distribution and is not prescribed. Also, if interacting boundary layer techniques are to be used, solution branching must be resolved by providing a downstream boundary condition for the boundary layer equations [58].

Mixing Methods

Mixing methods use a simplified analysis of the film cooling problem. The methods follow roughly the concepts of Stewart's [3] downstream mixing model. They are based on conservation laws and provide gross information rather than details of the injection process. This information is sufficient, however, to predict the aerodynamic loss of the cascade. Four mixing methods are used at the present time to provide estimates of turbine blade performance. Since these methods are described in references [20], [21] and [60], only the portions used in the present analysis will be discussed here.

Constant static pressure mixing. The simplest of the methods is the constant static pressure mixing model of reference [21]. The cooling jet row is modeled as a slot inclined to the surface. Assuming a perfect gas, the equations of conservation of mass energy and streamwise momentum, are applied to the system depicted in Figure 2. The outer boundary of the system is free to expand and contract so that the static pressure remains constant. The momentum of the jet normal to the primary flow is not considered in the analysis.

The governing equations are:

Conservation of mass

$$\frac{W_m}{W_u} = 1 + \xi \tag{1}$$

Conservation of energy

$$T_{t_m} = \frac{1}{1+\xi} (T_{t_u} + \xi T_{t_c}) \tag{2}$$

Conservation of streamwise momentum

$$V_m = \frac{1}{1+\xi} (V_u + \xi V_c \cos\theta_c) \tag{3}$$

Ideal gas laws

$$H_t = c_p T_t$$
$$P = \rho RT \tag{4}$$

Where the different pressures, temperatures and velocities are defined in Figure 2, and ξ is the ratio of the coolant to primary mass flow, W_c/W_u. Note that the specific heat, c_p, has been assumed constant throughout the flow field.

The change in total pressure, ΔP_t, between the upstream and mixed condition is determined using isentropic relations, and the assumption of constant static pressure.

$$\frac{\Delta P_t}{P_{t_u}} = \left[\frac{1 + \frac{\gamma-1}{2} M_m^2}{1 + \frac{\gamma-1}{2} M_u^2}\right]^{\frac{\gamma}{\gamma-1}} - 1 \tag{5}$$

where M is the Mach number and γ the ratio of specific heats. Again using the constant static pressure assumption, the Mach number of the upstream and coolant flows are calculated from the local pressure distribution on the outer boundary at the injection point

$$M_u^2 = \frac{2}{\gamma-1}\left[\left(\frac{P_t}{P}\right)_o^{\frac{\gamma-1}{\gamma}} - 1\right] \tag{6}$$

$$M_m^2 = \frac{2}{\gamma-1}\left[\left(\frac{P_t}{P}\right)_c^{\frac{\gamma-1}{\gamma}} - 1\right] \tag{7}$$

These Mach numbers are also used to determine the upstream and coolant velocities, V_u and V_c.

The mixed flow Mach number may be calculated using the definition of critical velocity ratio,

$$\left(\frac{V}{V_{cr}}\right)_o^2 = \left[\frac{V_m^2}{\frac{2\gamma R\, T_{t_m}}{\gamma+1}}\right] \tag{8}$$

and the relation between Mach number and critical velocity ratio.

$$M_m^2 = \frac{\frac{2}{\gamma+1}\left(\frac{V}{V_{cr}}\right)_m^2}{1 - \frac{\gamma-1}{\gamma+1}\left(\frac{V}{V_{cr}}\right)_m^2} \tag{9}$$

Combining equations (2), (3), (8) and (9), the mixed flow Mach number is expressed in terms of the upstream primary and coolant flow conditions as follows:

$$M_m^2 = \left[\frac{(\gamma-1)\, c_p (1-\xi)\left(T_{t_u} + \xi T_{t_c}\right)}{\left(V_u + \xi V_c \cos\theta\right)^2} - \frac{\gamma-1}{2}\right]^{-1} \tag{10}$$

Using the above relations for Mach numbers and the pressure distribution over the turbine blade, the total pressure change across each injection port may be calculated. The total loss due to the injection is the sum of the individual total pressure changes across each coolant port. This loss is added to the viscous, trailing edge injection and trailing edge blockage losses to arrive at an estimate of the cascade performance.

Composite mixing method. As presented in reference [21], the method consists of repeated application of static pressure mixing within a layer. In terms of computational efficiency and overall accuracy, it represents the best aerodynamic performance estimator of film cooled turbine blades to date.

The flow problem is depicted in Figure 3. The flow field is divided into three regions, two of which are mixing layers along the suction and pressure surfaces of the blade. The free boundaries of these surface layers correspond to the outer boundary in the static pressure mixing theory. The mass flow through each layer is the same at all times, so that the layer has to be considered to expand in the out plane direction to accommodate the injected flow. The percentage of the total flow considered to be within the layer is somewhat arbitrary, since the final performance results are only mildly dependent on this choice. Choosing the single layer mass flow based on twice the total amount of the expected injection flow in this layer has worked well for this investigator. The third part of the flow field is the main or primary flow, which forms an inviscid core in the flow passage between the mixing layers. The static pressure is considered constant across the mixing layer, and is controlled by the inviscid core flow pressure distribution which is taken as that on the blade surfaces without injection.

Various modified forms of the static pressure mixing have to be used depending on the injection location. Near the blade's leading edge most of the fluid is moving in the direction of the inlet flow. This direction is therefore adopted for stream-wise momentum rather than the direction tangent to the blade

surface. Along the blade surfaces the mixing theory is applied as it was previously presented. The contents of the two layers are mixed with the inviscid core flow at the trailing edge plane, and all three flows are assumed to be moving in the streamwise direction which is dictated by the trailing edge angle.

The aerodynamic performance of the blade row is calculated by considering the total pressure changes in the mixing layers. Starting at the leading edge, the change in total pressure is calculated as each injection port is encountered. Unlike the one dimensional mixing model, however, the upstream total pressure at a port is dependent on the previous total pressure changes in the layer due to upstream injection ports. At the trailing edge plane the layer and core flows are mixed using the constant static pressure method again. This provides a calculation of the change in total pressure through the blade passage due to the coolant injection. With this flow, a modified version of Stewart's method [3] which includes trailing edge injection, is used to complete the performance calculations.

The modified Stewart's method was developed by applying the general analysis of reference [3] to the flow depicted in Figure 4. Trailing edge injection was included in the method by incorporating additional terms in the conservation equations. The final equations for the downstream critical velocity ratio are given below.

Axial critical velocity ratio is

$$\left(\frac{V_a}{V_{cr}}\right)_2 = \frac{\gamma C}{\gamma+1} - \sqrt{\left(\frac{\gamma C}{\gamma+1}\right)^2 - 1 + \frac{\gamma-1}{\gamma+1}\left(\frac{V_u}{V_{cr}}\right)^2} \qquad (11)$$

where

$$C = \frac{\frac{\gamma+1}{2\gamma}\left[1-\frac{\gamma-1}{\gamma+1}\left(\frac{V}{V_{cr}}\right)_1^2\right]+\cos^2\alpha_1\left[\left(\frac{V}{V_{cr}}\right)_1^2(1-\delta_1-\theta_1)+A_{te}\left(\frac{\rho}{\rho_t}\right)_{te}\left(\frac{\rho_t}{\rho}\right)_1\left(\frac{V}{V_{cr}}\right)_{te}^2\right]}{\cos\alpha_1\left[\left(\frac{V}{V_{cr}}\right)_1(1-\delta_1)+A_{te}\left(\frac{\rho}{\rho_t}\right)_{te}\left(\frac{\rho_t}{\rho}\right)_1\left(\frac{V}{V_{cr}}\right)_{te}\right]} \tag{12}$$

Tangential critical velocity ratio is

$$\left(\frac{V_u}{V_{cr}}\right)_2 = \frac{\sin\alpha_2\left[(1-\delta_1-\theta_1)\left(\frac{V}{V_{cr}}\right)_1^2+A_{te}\left(\frac{\rho}{\rho_t}\right)_{te}\left(\frac{\rho_t}{\rho}\right)_1\left(\frac{V}{V_{cr}}\right)_{te}^2\right]}{\left(\frac{V}{V_{cr}}\right)_1(1-\delta_1)+A_{te}\left(\frac{\rho}{\rho_t}\right)_{te}\left(\frac{\rho_t}{\rho}\right)_1\left(\frac{V}{V_{cr}}\right)_{te}} \tag{13}$$

In the above relations, V/V_{cr} is critical velocity ratio, A_{te} is the area/unit span of the trailing edge injection slot, δ and θ are the boundary layer displacement and momentum thicknesses, α is the flow angle, and ρ is the fluid density. The subscripts 1, te, and 2 indicate flow properties at the trailing edge plane, trailing edge injection slot, and far downstream respectively.

Other Methods

Two methods for predicting aerodynamic losses were developed during the course of this analysis, but neither method produced acceptable performance estimates. They are presented, because some of their concepts are used in the analytical method of this report.

The first method was an inviscid flow analysis that included inviscid injection effects. The cascade loss was calculated by performing a numerical integration of the flow properties downstream of the blade row. This method did not succeed because the inviscid flow alone did not contain enough of the physics of the loss generating mechanisms. The mixing and viscous properties

of the fluid proved to be significant contributors to the losses, so that the performance estimates were characteristically too high.

The second method was suggested by Prof. Douglas E. Abbott of Purdue University, Lafayette, Indiana. He has had some unpublished success with it in predicting aerodynamic performance for single airfoils. The method is the same as used by Geller [45, 55] for predicting cascade flows. The basic analysis simulates the trailing edge flow separation as an injection of fluid out of the blade surface. The injection produces a constant pressure slip line over the separation. The simulated separation flow is interacted with a boundary layer calculation to locate the separation point on the blade surface. Lift and drag forces are then found by integrating the inviscid flow pressure distribution and boundary layer skin friction along the blade surface, assuming the skin friction to be zero in the separated regions.

When this technique was applied to the turbine cooling two problems arose. First, the coolant injection segments the boundary layer, making any continuous boundary layer calculations unfeasible. A boundary layer solution reported by Beavers and Stratford [61] may be adapted to provide a local similarity skin friction estimator, but any injection boundary layer interaction is ruled out if multiple cooling flow injection is to be studied. However, the interaction process may be rendered unnecessary if the separation point is assumed to coincide with the injection port. This is supported by experimental evidence [37]. Second, difficulty was also encountered in determining the components of lift and form drag from the pressure distribution integration, since the primary flow is turned by the cascade, and selection of reference velocity on which to base the lift and drag vectors is not obvious. With the usual choice of potential flow solution onset velocity as a reference, cases were encountered where positive form drag was calculated. The method still has some merit as an alternative to mixing theory, but further study is needed.

IMPROVEMENTS TO COMPOSITE MIXING MODEL

Of the various analytical methods studied, the composite mixing theory was found to give the best aerodynamic performance estimates for the widest range of injection locations and velocities. This method was therefore, selected as a basis for analysis of this report.

Improvements to the composite mixing method can be obtained by modifying two basic assumptions of the mixing theory. These assumptions are that the inviscid core flow which drives the mixing theory is unaffected by injection, and that the effects of injection on the boundary layer flow are negligible. By using the inviscid flow solution developed here, the injection effects were included in the mixing method. The detailed structure of the boundary layer with injection was found to be too complex to lend itself to analysis. However, by using a method similar to Geller [45], the effect of separation on the inviscid flow were modeled.

The analytical method used in this investigation was developed by incorporating these improvements into the mixing theory. The present method, therefore, consists of the composite mixing theory driven by an inviscid flow which includes the effects of injection and injection induced boundary layer separation.

POTENTIAL CASCADE FLOW PROBLEM FORMULATION USING DISTRIBUTED SINGULARITIES

To incorporate the improvements to the composite mixing theory described in the previous section, a means was needed to calculate an inviscid cascade flow with injection effects included. The integral-equation or distributed singularities solution was chosen for this calculation. It was selected because the solution can easily be adapted to calculate the injection effects on the inviscid flow. In addition the distributed singularities method has the potential to provide a very rapid solution since the cascade blade surface velocity distributions can be determined

without solving the complete flow field. References [42] through [49] and [65], provide detailed descriptions of the basic solution derivation, therefore only a brief outline will be given in this report.

General Cascade Potential Flow Problem

Referring to Figure 5, the cascade problem differs from the isolated airfoil problem in that the upstream and downstream velocities (V_I and V_E), are not the same. This is due to the flow circulation induced by the cascade across the entire flow field. However, the potential flow problem for the two dimensional cascade does follow the same line of though as that for a single airfoil with two modifications. First, the contributions of each of the airfoils making up the cascade have to be considered. Secondly, in the cascade problem, there is no physical counter part to the invariant free stream velocity in the single airfoil problem, but the idea of an undisturbed velocity is used to define an onset velocity which is constant throughout the flow field. This velocity is determined during the course of the iterative solution of the present method.

In the potential problem it is assumed that the flow is inviscid, steady, irrotational, and incompressible. With these assumptions the governing equations take the following form.

Continuity is,

$$\nabla \cdot \bar{V} = 0 \tag{11}$$

Conservation of momentum becomes simply Bernoulli's equation, and is used to determine pressures in the flow field.

$$c_p = \frac{P-P_{onset}}{\frac{1}{2}\rho V_{onset}^2} = 1 - \left(\frac{V}{V_{onset}}\right)^2 \tag{12}$$

where c_p is the pressure coefficient.

Boundary conditions at the cascade inlet and exit are,

$$\bar{V} \rightarrow \bar{V}_I \quad \text{as} \quad \bar{R} \rightarrow \infty \quad \text{upstream} \tag{13}$$

and $\bar{V} \rightarrow \bar{V}_E$ as $\bar{R} \rightarrow \infty$ downstream (14)

where $\bar{R}$ is the position vector from the cascade row. The other boundary condition is at the cascade body surfaces and specifies the normal velocity along these surfaces, F(t).

$$\bar{V} \cdot \bar{n}|_t = F(t) \quad \text{at} \quad \bar{R} = \bar{R}|_{body} \tag{15}$$

Solution of the Governing Equations

The flow velocity, $\bar{V}$, can be expressed as the summation of a constant onset velocity, $\bar{V}_{onset}$, and a variable disturbance velocity, v, which is not necessarily small

$$\bar{V} = \bar{V}_{onset} + \bar{v} \tag{16}$$

Since the onset velocity is constant throughout the flow field, the momentum is satisfied if the disturbance velocity $\bar{v}$, is described by the velocity potential function ϕ as follows,

$$\bar{v} = - \nabla\phi \tag{17}$$

By substitution into equation (16), the velocity vector becomes

$$\bar{V} = \bar{V}_{onset} - \nabla\phi \tag{18}$$

Using this definition in the continuity equation (11), Laplace's equation for the potential function is obtained

$$\nabla^2\phi = 0 \tag{19}$$

There are a number of real harmonic functions which satisfy the above equation, but it is more convenient to work with complex variables and take advantage of their compact notation and special algebraic manipulations.

The potential function (ϕ) is the real portion of the complex potential, C(z),

$$C(z) = \phi(z) + i\,\psi(z) \tag{20}$$

where z is a point in the complex plane

$$z = x + iy \tag{21}$$

In the above equations, i denotes the imaginary number ($\sqrt{-1}$), and ψ is the stream function. The coordinates of z in the complex plane are x and y. An analytic function may now be selected for C(z), so that the real part (ϕ) will satisfy Laplace's equation.

From ideal flow theory, two singular functions, namely source-sink and vortex, are known to be analytic throughout the flow field except at their origins. If $c = a + bi$ is the singularity location and r is the distance between c and z, the point of interest in the flow, these functions will have the following forms. The source-sink velocity potential is given as

$$\phi(z-c) = \text{Re}\,[C(z-c)] = s\ \ell n\ r \tag{22}$$

and the vortex velocity potential is written as:

$$\phi(z-c) = \text{Re}\,[C(z-c)] = -g\theta \tag{23}$$

where polar notation is used for the complex argument of the functions, so that

$$z-c = r\,e^{i\theta} \tag{24}$$

In the above equations, g and s are defined as the vortex and source-sink strengths. These potential functions may be written as a single function by defining a combined singularity strength.

$$k = (s + ig) \tag{25}$$

The complex potential then becomes

$$C(z-c) = k\ \ell n(re^{i\theta}) \tag{26}$$

and the combined velocity potential is:

$$\phi(z-c) = s\,\ell n(r) - g\theta \tag{27}$$

Laplace's equation is linear, and the sum of analytic function is also analytic. Using these facts, a solution may be formed by superposition of several singularity functions located throughout the flow region. For the single airfoil, the singularity functions are placed along the body surface to produce the disturbance potential, but for a cascade the simple sink-source and vortex potentials do not account for total effect of all the airfoils in the cascade row.

Referring to Figure 6, the complex y axis is aligned with the blade row, and the real x axis is perpendicular to it. Since the cascade is infinite, corresponding singularities on the cascade bodies located at distances S parallel to the y axis will have the same strength or density, k. The complex potential at any point in the flow field due to a line of these singularities can be written in the following series

$$C(z) = k[\ell n(z-c) + \ell n(z-c+iS) + \ell n(z-c-iS) + \ell n(z-c+2iS) + \ldots] \tag{28}$$

Combining terms with the same multiples of iS the series becomes

$$C(z) = k\{\ell n(z-c) + \ell n[(z-c)^2+S^2] + \ell n[(z-c)^2+(2S)^2] + \ldots\} \tag{29}$$

The components of the disturbance velocity (v_x, v_y) are found by taking the derivative of the complex potential. With a rearrangement of terms the resulting series takes the following form:

$$\frac{dC}{dz} = \frac{k\pi}{S}\left[\frac{S}{\pi(z-c)} + \frac{2\pi(z-c)}{S}\left(\frac{1}{\pi^2+\pi^2(z-c)^2/S^2} + \frac{1}{4\pi^2+\pi^2(z-c)^2/S^2} + \ldots\right)\right] \tag{30}$$

which is the same as the defining series for the complex hyperbolic cotangent.

The complex disturbance velocity, w, can now be written as a single function,

$$w = v_x - iv_y = \frac{k\pi}{S} \coth\left(\frac{\pi(z-c)}{S}\right) \tag{31}$$

and the complex potential may be found by integration.

$$C(z) = k \ln \left[\sinh \left(\frac{\pi(z-c)}{S}\right)\right] \tag{32}$$

This is the elementary potential for a cascade of singularities.

A body can be represented by distributing the source-sink and vortex singularities along its surface. The simplest way to distribute the singularities is to replace the body with polyhedron and use a line singularity of constant density over each segment of the polyhedron. The basic geometry of the problem is illustrated in Figure 6. To develop the line singularity formulation for the velocity function, one integrates the elementary velocity functions along the line segment on which they are distributed. A general segment lies along a coordinate line ξ oriented at an angle η to the x axis of the reference complex plane. The integration is between the bounds of the line segment c_1 and c_2. This discussion has concentrated on one body, but similar statements may be made for a cascade of bodies so that the integration takes place on the complex series derived previously in equation (31). The complex flow disturbance velocity, W, for a cascade can be expressed as follows:

$$W = \frac{k\pi}{S} \int_{c_1}^{c_2} \coth\left(\frac{\pi(z-c)}{S}\right) d\xi \tag{33}$$

where

$$c = ih + \xi e^{i\eta} \quad , \tag{33a}$$

$$dc = e^{i\eta} d\xi \quad , \text{ and} \tag{33b}$$

$$d\xi = e^{-i\eta} dc \tag{33c}$$

then

$$W(z) = \frac{k\pi}{S} \int_{c_1}^{c_2} \coth\left(\frac{\pi(z-c)}{S}\right) dc \tag{34}$$

Integration gives the following form of the complex velocity:

$$W(z) = -ke^{-i\eta} \ln \left[\frac{\sinh[\pi(z-c_2)/S]}{\sinh[\pi(z-c_1)/S]}\right] \tag{35}$$

The final form of the complex velocity for the two-dimensional problem requires another integration of the line singularity function in the out of plane direction to plus and minus infinity. This integration results in a factor of 2 and represents a plane surface singularity distribution:

$$W(z) = -2ke^{-i\eta} \ln \left[\frac{\sinh[\pi(z-c_2)/S]}{\sinh[\pi(z-c_1)/S]}\right] \tag{36}$$

Resolving the Far Stream Boundary Conditions

With the disturbance velocity given by equation (36), which satisfies the governing equation, it is necessary to have a closer look at the far upstream and far downstream flows in order not to violate the cascade inlet and exit boundary conditions. At a far stream station, the cascade singularity distribution would appear as a row of point sink-source and vortex singularities.

The disturbance velocity at the far upstream and downstream boundary conditions is determined by taking the limit of equation (31) as

$$\begin{aligned} &\frac{\pi}{S}(z-c) \to +\infty \qquad \text{far downstream} \\ &\frac{\pi}{S}(z-c) \to -\infty \qquad \text{far upstream} \end{aligned} \tag{37}$$

and by replacing k by $K = \Sigma + \Gamma i$ in which Σ and Γ are the concentrated source-sink and vortex density of a cascade blade. After taking the limit, the upstream disturbance velocity is found to be

$$v_{x_{-\infty}} = 0 \quad , \quad v_{y_{-\infty}} = \frac{\Gamma\pi}{S} \tag{38}$$

Similarly the downstream disturbance velocity is given as

$$v_{x_{+\infty}} = 0 \quad , \quad v_{y_{+\infty}} = -\frac{\Gamma\pi}{S} \tag{39}$$

Now from ideal fluid flow, the circulation, Γ_{cir}, is given by the line integral of the tangential velocity component around the body and can be related to the vortex density as follows:

$$\Gamma_{cir} = \oint \bar{V} \cdot d\bar{t} = 2\pi\Gamma \tag{40}$$

Using equation (40) in equations (38) and (39), the following relationships are obtained.

$$v_{y_{-\infty}} = \frac{\Gamma_{cir}}{2S} \tag{41}$$

$$v_{y_{+\infty}} = -\frac{\Gamma_{cir}}{2S} \tag{42}$$

These disturbance velocity components, $v_{y-\infty}$ and $v_{y+\infty}$, are shown in the vector diagrams of Figure 5, as V_{up} and V_{down} respectively.

Using these diagrams, the following relations can be written:

$$\alpha_{inc} = \alpha_I - \beta \tag{43}$$

$$\Delta\theta = \alpha_I - \alpha_E \tag{44}$$

where α_{inc} is the incidence angle of attack, α_I is the inlet flow angle, and β the stagger angle of the cascade. Also $\Delta\theta$ is the flow turning angle and α_E is the exit flow angle.

Using equations (40) and (41) for V_{up} and V_{down}, and the vector diagrams of Figure 5, the following relations are obtained.

$$\alpha_I = \tan^{-1}\left[\frac{V_{onset}\sin\alpha + \frac{\Gamma cir}{2S}}{V_{onset}\cos\alpha}\right] \tag{45}$$

$$\alpha_E = \tan^{-1}\left[\frac{V_{onset}\sin\alpha - \frac{\Gamma_{cir}}{2S}}{V_{onset}\cos\alpha}\right] \tag{46}$$

where α is the angle of attack of V_{onset} and is negative as shown in Figure 5.

In the solution being presented, inlet flow conditions are given. Equation (45) is then used iteratively with the velocity solution, to determine the values of V_{onset}, α, and Γ_{cir}. Once a velocity solution which is consistent with the inlet conditions, is obtained, equations (45), (42) and (43) are used to calculate α_E, $\Delta\theta$, and α_{inc}. Note that if both α_I and α_E are given the velocity solution parameters (α, Γ_{cir}, and V_{onset}) can be found without iteration.

Resolving the Cascade Body Surface Boundary Condition

The cascade body surface boundary condition is the final requirement to be satisfied by the solution. From this boundary condition comes the integral equation to be solved. Recalling equation (15), the boundary condition was written in general form as

$$\bar{V}\cdot\bar{n}_{|t} = F(t) \qquad \text{at} \quad \bar{R} = \bar{R}_{|body}$$

Substituting equation (18) for $\bar{V}$ into the above equation the following relation is obtained

$$\nabla\phi\cdot\bar{n}_{|t} = \bar{V}_{onset}\cdot\bar{n}_{|t} - F(t) \tag{47}$$

Using the polyhedron approximation of the blade, control points are selected at the mid-points of each of the sides of the polyhedron as shown in Figure 7. The surface boundary condition is satisfied at each of these control points. The disturbance velocity at the control points is the total effect of all the surface singularities along the polyhedron sides.

$$\bar{v} = v_t - iv_n = -\nabla\phi = \sum_{i=1}^{n} W(z) \tag{48}$$

Substituting equation (36) for W gives:

$$\bar{v} = \sum_{m=1}^{n} -2k\, e^{-i\eta}\, \ell n\, \left[\frac{\sinh[\pi(z-c_{m+1})/S]}{\sinh[\pi(z-c_m)/s]}\right] \tag{49}$$

Substituting this into equation (47), the following relation is obtained:

$$\sum_{m=1}^{n} -2k_m(t)\, e^{-i\eta}\, \ell n\, \left[\frac{\sinh[\pi(z-c_{m+1})/S]}{\sinh[\pi(z-c_m)/S]}\right] = \bar{V}_{onset}\cdot\bar{n}\Big|_j - F_j(t) \tag{50}$$

Where j is an index that identifies the control point at which the boundary condition is being evaluated. It should be noted that surface singularity of equation (36) was derived in a coordinate system aligned with its surface. When this relation is used in the integral equation (50) care must be taken to resolve the disturbance velocity components into the coordinate system of point in the flow field where the flow velocity is to be calculated.

By writing relations similar to equation (50), for each control point on the polyhedron, a system of n equations will result. The solution to these equations gives the singularity density, $k_j(t)$, at the control points.

$$k_j(t) = s_j(t) + i\, g_j(t) \tag{51}$$

The above derivation gives the discrete approximation of the integral equation. The integral equation form may be recovered may be recovered by using an infinite sided polyhedron to represent the blade:

$$\int \nabla\, k(t)\, f(t) \cdot n(t)\, dt = \bar{V}_{onset} \cdot \bar{n}(t) - F(t) \tag{52}$$

where f(t) is the known singularity function and k(t) is to be determined.

The value of the function F(t) is normally taken to be zero for the solid boundary case. If injection occurs, F(t) or $F_j(t)$

takes on the value of the normal velocity component of the fluid injected at the particular location on the blade surface.

After the singularity density distribution has been found, the velocity at any point in the flow field may be calculated using the following relation:

$$V_x + iV_y = V_{onset} \cos\alpha + V_{onset} \sin\alpha + v_x + iv_y \qquad (53)$$

Where v_x and v_y are the components of the disturbance velocity $\bar{v}$ which can be determined from equation (49).

DISCUSSION OF SOLUTION TECHNIQUES FOR THE POTENTIAL FLOW PROBLEM

Several solution techniques exist for developing the singularity distributions. In most of the methods, which use a combination of source-sink and vortex densities, the singularity distributions are considered to be independent of one another. The simplest techniques for finding the distributions assumes constant source-sink density over all the elements. The values of source-sink density for each element are found by solving the system of equations similar to equation (50) for each element. The vortex density is determined from the Kutta condition or a similar requirement on the flow leaving the trailing edge. This technique will mainly be used for comparisons and is therefore, referred to as the base method. By using more complex, element geometries and singularity distributions, higher order accurate solutions than the base method may be formulated [47], [51].

Bristow [50] developed a method for single multi-body airfoils. In his method the source-sink and vorticity distributions are found using a density minimization function, which makes them interdependent. Several improvements over the base method are accomplished by using this technique. Although both methods are first order in error resoltuion the minimized solution has better accuracy. The comparison problem of a single circular

cylinder without circulation was studied, and solution errors are compared at the peak velocity point 2 1/2 radii above the cylinder. As can be seen in Figure 8, the minimized method produces the same error level as the base method with less than half the number of elements being used to approximate the cylinder. Another advantage of the minimization solution is that it can easily handle very thin geometries. The base method cannot analyze these geometries without reducing element size in the thin region. Also the solution in high velocity gradient areas (i.e. airfoil leading edges) is improved by minimization. Finally, the base method is very sensitive to the relative size of adjacent elements. No element should be double the size of element next to it, or a spike in the solution curve will result at the element. The minimized method is less sensitive, but violation of the element size criteria will still produce erratic solutions. Because of its simplicity and improvements over the base method, Bristow's technique was adapted to the cascade problem and used in the analytical study.

SINGULARITY DENSITY MINIMIZATION SOLUTION FOR CASCADES

The minimization method uses an expanded form of equation (53) as a starting point. Two mutually perpendicular velocity components at any point i in the flow field are:

$$V_{T_i} = V_{onset} \cos(\theta_i - \alpha) + \sum_{j=1}^{n} A_{s_{ij}} s_j + \sum_{j=1}^{n} A_{V_{ij}} g_j \qquad (54)$$

$$V_{N_i} = -V_{onset} \sin(\theta_i - \alpha) + \sum_{j=1}^{n} B_{s_{ij}} s_j + \sum_{j=1}^{n} B_{V_{ij}} g_j \qquad (55)$$

The angles to the reference coordinate system of V_{T_i} and V_{onset} are θ_i and α, respectively. The source-sink singularity distribution, s_j, and the vortex singularity distribution, g_j, are to

be determined, however the general forms of these distributions must be specified before solution is initiated. Using these specified forms and the given geometry of the problem, the influence coefficients (A_s and B_s) due to the source-sink singularities and the influence coefficients (A_v and B_v) due to the vortex singularities, may be determined. If equation (55) is written for the control points of the body, the system of equations that results in equivalent to the body surface boundary condition previously described by equation (50) with V_{N_i} replacing $F_j(t)$. In matrix form, the system is expressed as:

$$[V_{N_i}]_{nx1} = [-V_{onset} \sin(\theta_i - \alpha)]_{nx1} + [B_{s_{ij}}]_{nxn} [s_j]_{nx1} + [B_{v_{ij}}]_{nxn} [g_j]_{nx1} \quad (56)$$

Solving for the source-sink strength distribution gives:

$$[s_j]_{nx1} = [B_{s_{ij}}]^{-1}_{nxn} [V_{N_i} + V_{onset} \sin(\theta_i - \alpha)]_{nx1} - [B_{s_{ij}}]^{-1}_{nxn} [B_{v_{ij}}]_{nxn} [g_j]_{nx1} \quad (57)$$

Defining the following new variables

$$[\beta_k]_{nx1} = [B_{s_{ij}}]^{-1}_{nxn} [V_{N_i} + V_{onset} \sin(\theta_i - \alpha)]_{nx1} \quad (58)$$

$$[C_{k\ell}]_{nxn} = [B_{s_{ij}}]^{-1}_{nxn} [B_{v_{ij}}]_{nxn} \quad (59)$$

and using these variables [equations (58) and (59)], equation (57) can be written as follows:

$$[s_k]_{nx1} = [\beta_k]_{nx1} + [C_{k\ell}]_{nxn} [g_\ell]_{nx1} \quad (60)$$

A density function which is to be minimized, can now be formed in which the only unknowns are g_k, the strengths of the vortex distribution.

$$G[s_k(g_k),\ g_k] = \sum_{k=1}^{n} [\Delta_{s_k} s_k^2 + \Delta_{v_k} g_k^2] \tag{61}$$

where Δ_s and Δ_v are the areas over which a particular singularity has influence. The source-sink strengths (s_k) are eliminated with the use of equation (60).

In order to minimize the function G and also to evaluate the influence coefficients, the form of the singularity distribution must be known. The form of the source-sink singularity distribution, s_k, is assumed to be simply a constant over each element. However, since minimization involves taking derivatives, the function, G, should be continuous and differentiable with respect to its independent variables, g_k. To assure this, the vortex strength distribution, g_k, is selected to be linear over each element and continuous around the body. Referring to Figure 7, this implies that the final value of g on one element i is the initial value of g on the next element, i+1. Assuming the elements and body points are numbered as in Figure 7 (i.e. starting at the lower trailing edge and moving in a clockwise direction), a discontinuity in the vortex strength distribution will occur for closed body at the trailing edge, unless the value of g_1 is made equal to the value of g_{n+1}. This also helps to keep the solution bounded in the trailing edge region.

With the forms of singularity strengths known, the influence coefficients and distribution areas may be calculated. Evaluation of the influence coefficients require considerable algebraic manipulation and lengthy equations. The derivation of coefficients is therefore presented in an Appendix. The distribution areas, the Δ's in equation (61), are calculated as a fraction of the total perimeter of the body. If each element is ℓ_k long, the following relations can be written:

$$\Delta_{s_k} = \ell_k / \sum_{k=1}^{n} \ell_k \tag{62}$$

$$\Delta_{v_k} = \begin{cases} (\ell_k + \ell_{k-1})/2 \sum_{k=1}^{n} \ell_k & \text{for } k \neq 1 \\ (\ell_1 + \ell_n)/2 \sum_{k=1}^{n} \ell_k & \text{for } k = 1 \end{cases} \tag{63}$$

The final step of the solution is the incorporation of a requirement on how the flow is to leave the trailing edge of the body. For the sharp trailing edge airfoil shape, the Kutta condition, that the flow leave the trailing edge smoothly, is the obvious choice. However, a turbine blade has a round trailing edge, and no clear cut condition exists. In the solution being presented, the trailing edge geometry of the blunt ended airfoil is ignored. The problem is solved as an open body as depicted in Figure 7. This is justified by real flow considerations that the rounded trailing edge will be submerged in a viscous separation wake and therefore has little influence on the inviscid flow. For a trailing edge flow requirement, zero normal flow velocity is maintained on the bisector of the trailing edge angle at a point downstream. This point is taken at a distance which is one-tenth the length of the smallest of the two elements adjacent to the trailing edge. This is the same criteria used by Bristow [50], and is also compatible with the Kutta condition for sharp trailing edges. Physically, this condition may be construed as requiring a straight wake leaving the blade parallel to the trailing edge bisector. In order to implement this condition, the solution must remain finite or bounded in the trailing edge region. To assure this, additional requirements are made that the values of the singularity strength on both sides of the trailing edge be equal.

Mathematically the trailing edge conditions act as constraints on the singularity density function G. The zero normal flow velocity requirement is written as:

$$V_{N_{TE}} = -V_{onset} \sin(\theta_{TE}-\alpha) + \sum_{j=1}^{n} B_{s_{TEj}} s_j + \sum_{j=1}^{n} B_{v_{TEj}} g_j = 0 \tag{64}$$

Substituting equation (60) for s_j, equation (64) becomes

$$-V_{onset} \sin(\theta_{TE}-\alpha) + \sum_{j=1}^{n} B_{s_{TEj}} \left(\beta_j + \sum_{k=1}^{n} C_{jk}\, g_k\right) + \sum_{j=1}^{n} B_{v_{TEj}}\, g_j = 0 \qquad (65)$$

or in matrix notation, it takes the following form.

$$V_{onset} \sin(\theta_{TE}-\alpha) = [B_{s_{TEj}}]_{1xn} [\beta_j]_{nx1}$$

$$[B_{s_{TEj}}]_{1xn} ([C_{jk}]_{nxn} [g_k]_{nx1} + [B_{v_{TEj}}]_{nxn} [g_j]_{nx1}) \qquad (66)$$

The trailing edge requirement for the source-sink singularity strengths is:

$$s_1 = s_n \qquad (67)$$

Using equation (60), equation (67) becomes,

$$\beta_1 - \beta_n = [C_{nk} - C_{1k}]_{1xn} [g_k]_{nx1} \qquad (68)$$

The same requirement when applied to the vortex singularity strengths is written as

$$g_1 = g_k \qquad (69)$$

and was already enforced by the selection of a piecewise continuous vortex distribution.

The problem can now be set up as the minimization of the density function, G, subject to two constraints. The method of Lagrangian multipliers is employed.

$$Q = G + \lambda_1(\text{eqn. } 66) + \lambda_2(\text{eqn. } 68) \qquad (70)$$

where λ_1 and λ_2 are the Lagrangian multipliers. Expanding equation (70), the following is obtained.

$$Q = \{[\Delta_{s_i}]_{1xn} [([\beta_i]_{nx1} + [C_{ik}]_{nxn} [g_k]_{nx1})^2]_{nx1}$$

$$+ [\Delta_{v_i}]_{1xn} [g_k^2]_{nx1}\} + \lambda_1\{[B_{s_{TEj}}]_{1xn} [\beta_i]_{nx1}$$

$$+ [B_{s_{TEj}}]_{1xn} [C_{ik}]_{nxn} [g_k]_{nx1} + [B_{v_{TEj}}]_{1xn} [g_j]_{nx1}$$

$$- V_{onset} \sin(\theta_{TE}-\alpha)\} + \lambda_2\{[C_{nk}-C_{1k}]_{1xn} [g_k]_{nx1}$$

$$- (\beta_1 - \beta_n)\} \qquad (71)$$

In functional form, equation (71) may be written as

$$Q = Q(g_1, g_2, g_3, \ldots g_n, \lambda_1, \lambda_2) \qquad (72)$$

To find the minimum value of Q, derivatives are taken with respect to each of the independent variables and set equal to zero.

$$\frac{\partial Q}{\partial g_1} = \frac{\partial Q}{\partial g_2} = \frac{\partial Q}{\partial g_3} = \ldots = \frac{\partial Q}{\partial \lambda_1} = \frac{\partial Q}{\partial \lambda_2} = 0 \qquad (73)$$

The above relations form a system of linear equations, and are solved for the value of the independent variables ($g_1 \ldots g_n$, λ_1, λ_2). This gives the minimum Q and the corresponding constrained singularity density distributions.

$$\begin{bmatrix} \\ D \\ \\ \end{bmatrix} \begin{bmatrix} g_1 \\ g_2 \\ \vdots \\ g_n \\ \lambda_1 \\ \lambda_2 \end{bmatrix} = \begin{bmatrix} \\ E \\ \\ \end{bmatrix} \qquad (74)$$

where D is a square coefficient matrix with dimension n+2 and E is column constant matrix with dimension n+2. Details of the coefficient and constant matrices (D and E) are worked out in the Appendix.

Analysis of equation (74) brings out some important facets of the formulation. The coefficient matrix, D, is dependent totally on the geometry of the problem. The constant matrix, E, is a function of the given values of the injection velocity over the surface and the angle of attack of the onset flow, α. Once the coefficient matrix has been inverted, an inviscid flow solution algorithm has essentially been created for the body geometry under study. Solutions for varying angles of attack and injection configurations become simply a matter of matrix multiplication.

The solution to equation (74) gives the vortex strength distribution. This is substituted in equation (60) which yields the source-sink strength distribution. These distributions are substituted into equation (54) using the control points on the body surface to give the tangential velocity on the body. The tangential velocity is integrated around the body giving the circulation. The circulation is used in equation (45) so that the far upstream boundary condition for the cascade problem is satisfied. The specified normal velocities and the calculated tangential velocities are used in the momentum equation formulation of the pressure coefficient to give the pressure distribution over the body. Finally, equations (54), (55) and the pressure coefficient may be used to determine the velocity and pressure at off body points in the flow field.

COMPRESSIBILITY CORRECTION

The integral equation solution gives only the potential or ideal flow through the cascade. In a turbine blade row, local Mach numbers may approach unity because of the high camber of turbine airfoils, the reduction of flow area in the blade passages, and the favorable pressure gradient across the row.

Compressible effects become significant as a Mach number of 0.5 is exceeded, so that a correction to the turbine potential flow solution is needed.

Several techniques of varying levels of sophistication and computational effort are available to provide these corrections. The tangent gas or Karman-Tsien compressibility correction is one of the simpler methods, and was used in the solution being presented. The method is well known, and any text on gas dynamics contains a discussion on it (i.e., see Shapiro [60]). The tangent gas correction is presented below as it was used.

For the method a correction factor is formulated

$$\lambda = \frac{M_{ref}^2}{(1+\sqrt{1-M_{ref}^2})} \tag{75}$$

M_{ref} is the Mach number of the flow which has the same thermodynamic properties at the point of tangency between the ideal equation of state and an approximate linear equation of state. For this solution, M_{ref} was the Mach number of the potential flow onset velocity. The compressible velocity is found from the following relation:

$$\left(\frac{V}{V_{ref}}\right)_{comp} = \frac{\left(\frac{V}{V_{ref}}\right)_{inc} (1-\lambda)}{1 - \lambda\left(\frac{V}{V_{ref}}\right)_{inc}^2} \tag{76}$$

where the subscripts comp and inc indicate compressible and incompressible. The incompressible velocity ratios are obtained from the potential flow solution. Critical velocity ratios are then found using the compressible velocity of equation (76). The remaining flow properties can be determined by using isentropic relations. The compressible pressure coefficient is found to be:

$$C_{p_I} = \frac{P-P_I}{\frac{1}{2}\rho V_I^2} = \frac{2}{\gamma M_I^2}\left[\left\{1+\frac{\gamma-1}{2}M_I^2\left(1-\left(\frac{V}{V_I}\right)_{comp}\right)\right\}^{\frac{\gamma}{\gamma-1}} - 1\right] \tag{77}$$

The ratio of specific heats (γ) of the actual flow is used in the relation, although $\gamma=-1$ would be in accordance with the Karman-Tsein correction. The actual flow specific heat ratio, however, gave results which were in better agreement with experimental findings.

INJECTION FLOW

A method of calculating the injection velocity was needed. The problem was modelled as a total pressure reservoir discharging into a known static pressure through an orifice. The flow parameters are the same as those depicted in Figure 2 for the mixing theories. Using isentropic relations, the injection flow Mach number is:

$$M_c^2 = \frac{2}{\gamma-1}\left[\left(\frac{P_{t_c}}{P_o}\right)^{\frac{\gamma-1}{\gamma}} - 1\right] \tag{78}$$

The injection Mach number, M_c, is used to calculate the injection critical velocity ratio as follows:

$$\left(\frac{V_c}{V_{cr}}\right)^2 = \frac{\frac{\gamma+1}{2} M_c^2}{\left(1 + \frac{\gamma-1}{2} M_c^2\right)} \tag{79}$$

where $$V_{cr}^2 = \frac{2\gamma}{\gamma+1} R T_{t_c} \tag{80}$$

and R is the gas constant of the coolant.

Using the above relations the ideal coolant velocity, V_c, is determined. In order to obtain real flow velocities, experimentally determined discharge coefficients, C_D, for the injection row were used.

$$C_D = \frac{W_{c_{measured}}}{(\rho V A)_{c_{ideal}}} = \frac{V_{c_{actual}}}{V_{c_{ideal}}} \tag{81}$$

Areas equivalent to the total port areas of the injection rows are calculated so that injection mass flow estimates can be made using the two-dimensional model problem. This is done by determining a slot width which gives the same injection area per unit span as the row of ports. This slot width is then used in the analytical solution.

SEPARATION MODEL

The injection induced separation model is schematically represented in Figure 9. The model is similar to that used by Geller [45] and [55], to approximate trailing edge separations in cascades.

The separation region is considered to lie under a constant pressure slip line. This line starts at the injection port and continues downstream at the injection induced pressure level. The constant pressure condition is enforced by using pseudo-injections downstream of the coolant port. The potential flow pressure coefficient along the boundary of the separation is

$$C_{p_{sep}} = 1 - (V^2_{N_{sep}} + V^2_{T_{sep}}) \tag{82}$$

Where $V_{N_{sep}}$ is the actual or pseudo-injection velocity, and $V_{T_{sep}}$ is the tangential velocity along the surface which is primarily affected by the geometry of the flow field. The inviscid flow field velocity, V_{inv} is tangential to the body and separation regions at all times. The inviscid pressure coefficient can therefore be written as:

$$C_{p_{inv}} = 1 - V^2_{inv} \tag{83}$$

Along the slip line of the separation region, the inviscid and separation pressures are equal, so that the pseudo-injection, $V_{N_{sep}}$, can be determined as:

$$V^2_{N_{sep}} = V^2_{inv} - V^2_{T_{sep}} \tag{84}$$

The pseudo-injection velocity, V_N, will be real only if the injection induced pressure is less than the pressure due to the flow field geometry alone. Physically this implies that pressure due to the blade passage geometry must be greater than the injection induced pressure in order to keep the separation region contained. If it is not, the separation region will expand into the inviscid stream. Therefore, a separation region cannot continually extend downstream in a locally favorable pressure gradient.

Incorporation of the separation model requires alterations in the potential flow solution. First the model, which adds an iterative loop to the solution procedure, acts as an additional constraint. This separation constraint is usually compatible with the basic solution except when the separation extends to the trailing edge. In that case an inconsistency may arise between the model and the straight trailing edge wake constraint of the potential solution. When this occurs, the solution converges to a solution which honors the separation model constraint. Second, if the pseudo-injection velocities are chosen to be directed outward from the cascade body surface, the mass flow build-up results in increased flow velocities. Since the pressure coefficient is dependent on the magnitude of velocity and not its direction, the pseudo-injection mass flow build-up problem was partially eliminated by alternating the direction of pseudo-injections into and out of the blade. The alternating pseudo-injections did not change the shape of the inviscid velocity distribution curve from the case when the pseudo-injections were all outward, but it did reduce the inviscid velocity levels. It was noticed that a solution instability was encountered sometimes, if the separation region extended to the next downstream injection port. Logic had to be added to the computer program to prevent this by insuring that the pseudo-injection just upstream of the second port was directed into the blade.

MASS FLOW CORRECTIONS

Two mass flow corrections are required in the analytical solution. First in the real turbine cooling problem, the sum of the primary and injection mass flow will remain constant, since the injection flow is taken from the main flow in the compressor. To include this in the analysis, the calculated incompressible injection mass flow of the solution is used to correct the inlet flow condition. However, the injection velocity calculation and inlet flow correction lag the cascade blade pressure distribution calculation so that iteration is necessary in order to produce consistent solution. The second mass flow correction is needed to alleviate discrepancies between the mass flow calculated using injection parameters and that indicated by an integration of the analytical flow conditions at a downstream station. These discrepancies arose because large approximating blade elements, which did not properly model the injection row, were used in the potential flow solution to reduce computational effort. The use of the large elements resulted in a higher mass flow and a correspondingly higher average velocity out of the blade row than should exist in actuality. However, the real injection row flow parameters were used to calculate the actual injection mass flows so that the potential flow solution mass flow, and average velocity could be corrected to their proper values.

COMPARISON OF PRESENT SOLUTION WITH OTHER ANALYTICAL SOLUTIONS AND EXPERIMENTAL RESULTS

The ability of the analytical solution to calculate cascade flows was investigated by performing a series of comparisons with other analytical solutions and experimental results. These comparisons were carried out as the solution was developed, so that weaknesses in the present solution could be isolated.

First the potential or ideal cascade flow calculations were verified by using Gastelow's exact solution [62] which is based on the use of conformal transformations. Figure 10 shows the blade shape analyzed and approximating polyhedron, which

was used in the analysis. The vertices of the polyhedron were generated by patching two spline curve fits of the blade pressure and suction surfaces together with the circular segment forming the leading edge. The pressure coefficients obtained using the two methods are shown in Figure 11. It can be observed that the present solution is in good agreement with the exact solution everywhere, except at three locations. Discrepancies did occur near the trailing edge and just aft of the leading edge on both the suction and pressure sides of the blades. The major contributor to these errors was found to be the curve fit approximating polyhedron. Referring back to Figure 10, it can be seen that the leading edge errors occur in the transition region from small to large elements where some elements are nearly double the size of their neighbors. This violates the element sizing requirements of the analytical method and can therefore, explain the errors in that region. In the trailing edge region, errors can be attributed to the failure of the blade curve fit approximation to capture the cusped trailing edge of the actual airfoil.

Next, results from the present solution were compared to the experimental low speed cascade data of reference [63]. The cascade airfoil had a blunt leading edge, a symmetric thickness distribution with a maximum thickness ratio of 0.1, and a cusped trailing edge. Lift curves are shown in Figure 12 for two cascade solidities. Analytical and experimental surface pressure distributions are plotted in Figure 13. From these figures it can be concluded that the agreement between experimental and analytical results is good. The pressure distribution obtained using the base singularity method is also shown in Figure 13. It is clear that the present minimization method gives better results than the base method in the leading edge high velocity gradient region and in the thin trailing edge area of the cascade airfoil.

The final test of the present method was a cascade of typical turbine blades shapes as shown in Figure 14. Using this blade

blade shape, the first comparison with experimental data of reference [64] is shown in Figure 15. The comparison shows that the present method does a fair to good job of predicting the cascade flow with the largest error occurring at the pressure side trailing edge. This error indicates that the trailing edge geometry needs to be better represented and/or that a different constraint on the trailing flow should be used. In order to explore the validity limit of the compressible flow correction, a comparison was made with reference [66]. The turbine blade shape was the same as in the previous comparison, but the cascade stagger and spacing are slightly different. Figure 16 shows that, as expected, the correction became less effective as Mach numbers increased. It was determined that the blade surface velocity should not exceed 85% of the critical velocity if good results are to be achieved. Analytical results were also obtained for the same cascade with 13.4 percent coolant mass flow injection and the coolant total pressure equal to the primary flow. The change in the blade pressure distribution due to the injection is shown in Figure 17. Although no experimental data is available for direct comparison, the flow near the injection rows was found to be similar to the qualitative description of reference [37].

With confidence in cascade flow solution established, the validity of the total aerodynamic performance calculation procedure was studied. The procedure was verified by comparing the analysis with the data from the experimental test program of reference [16]. Figures 17 and 18 show that the analytical solution is in good agreement with the experimental data. The solution appears to give better results for injection from the pressure side than from the suction side. The largest discrepancies between experimental and analytical results are observed for cases involving injection from either side of the blade near the trailing edge. As shown in Figure 20, the results obtained in using the present method are also compared to the composite mixing method of reference [21], which does not consider injection and separation effects on the invisid stream. Figure 20 indicates

that the two methods have about the same error level when compared to experimental data [16]. Multiple injection computational results are compared with experimental data and the composite mixing model in Figure 21. This comparison shows the present method to be better than the composite mixing method at the lower levels of injection mass flow and decidedly worse for injection mass flows above 20 percent. These multiple injection results are primarily of academic interest only since the maximum injection mass flow in a real turbine is of the order of 10 percent.

After the completion of this comparison study, a statement on the capabilities of the present method may be made. First the present method does a good job of predicting potential and compressible cascade flows with and without injection. Second, when used to estimate film cooled cascade aerodynamic losses, the present solution works well as long as high injection rates, sonic injection, and injection induced total separation (i.e. past the blade trailing edge) are avoided. Last, although the error levels of the present method are equal to those of the composite mixing model, the present analysis should predict injection mass flow levels better. Occurrences of undesirable flow phenomena such as injection induced separation, sonic injection, and injection-primary flow interaction which cause large cascade losses can also be predicted using the present analysis. Using this information, film cooled turbine blade designs may be improved.

DESIGN STUDY USING THE PRESENT METHOD

The final version of the analytic solution can be used as a design tool. To demonstrate this and also to gain further insight into the aerodynamics of the film cooling process, a design analysis is made. Since a considerable amount of data was already available for the turbine of reference [16], a redesign of its cooling ports configuration was the problem considered.

Cooling Configuration

Port locations are determined by considering the surface pressure distribution, manufacturing capabilities, and heat transfer

characteristics. There are several reasons to avoid leading edge injection, although experimental and analytical results have shown reasonable aerodynamic performance. First leading edge injection is highly disruptive to the flow field, inducing separation and tending to extend the stagnation flow region over a larger area of the leading edge. This can be partially attributed to the use of perpendicular injection, which is due to the inability to construct ports with small injection angles in the leading edge region. Leading edge injection also requires a high chamber pressure to produce outward injection velocities. Furthermore unless the port row is positioned such that cooling flow is divided in tow directions, some portion of the leading edge will not be protected by the cooling film. The cooling of the blade leading edge can be achieved using other methods such as jet impingement on the inner surface.

Injection rows should not be located in areas where the local pressures are unfavorable, since separation is likely to result. Referring to Figure 17, it can be seen that locations between 5-10 percent of the pressure surface and 35-45 percent of the suction surface would be poor choices for port locations. Injection from the aft portion of the blade suction side should also be limited, since high injection velocities and performance losses can result due to the low pressures in that region.

Two final design criteria are discussed in the following. First, injection rows should occur in pairs so that the ports may be staggered providing better film coverage. Second in the thin region of the trailing edge, manufacturing of the injection ports is difficult, and the region is also structurally weak. Pin cooling can be used in the region, and the cooling fluid injected out of the trailing edge.

Using the above information, a turbine blade design was made and is depicted in Figure 22. Impingement cooling is used at the leading edge. Injection occurs between 15-30 percent and 55-70 percent of the surface distance on both sides of the blade, using pairs of injection rows. These rows are modeled as slots which have widths equal to 0.00735 units of blade chord. Film

cooling injections are all vectored at the same angle to the local contour. A transpiration insert is used for the 55-70 percent injection on the suction side. This insert has a low discharge coefficient which keeps the injection velocities down, and a large injection area which allows good film coverage. Transpiration injection occurs over the total area of the insert and is at 90 degrees. The trailing edge is cooled using the pin cooling and trailing edge injection combination. The trailing edge injection is from a slot 0.0055 units of chord wide and is directed along the trailing edge bisector. The film cooling, transpiration and trailing edge injection discharge coefficients are 0.7, 0.05, and 0.7 respectively.

Parameter Variation

The cooling blade design was analyzed for the effects of variation in injection mass flow, angle, and total temperature. The results are displayed in terms of primary air efficiency, which is equal to the ratio of actual kinetic energy output of the blade row to the ideal kinetic energy of primary flow alone. The thermodynamic efficiency, which represents the ratio of actual kinetic energy of the blade row to the summed ideal kinetic energies of the primary and injection flows was also calculated and displayed.

Injection mass flow was varied by specifying different internal total pressures. The film cooling injection angle and coolant total temperature ratio were held constant at 30 degrees and 1.0 respectively. Figure 23 shows the results for this case. Positive or outward injection from all coolant rows was not achieved until a coolant total pressure ratio of 0.99 was reached. Primary air efficiency shows a steady increase which seems to be proportional to the injection mass flow. Thermodynamic efficiency shows a slight decrease until the injection mass flow reaches 10 percent. It then starts to decrease at a greater rate. These results are a consequence of the formulation of the performance parameters. The primary air efficiency contains a multiplier in the form of a ratio of total mass flow to primary mass flow. As injection increases, total mass flow increases and

primary mass flow decreases which causes the multiplying ratio to become larger. An increase in the injection mass flow results in a decrease in the thermodynamic efficiency because the denominator, contains the ideal kinetic energy which increases with injection velocity, while the numerator remains relatively constant.

Variations of the two efficiencies with injection angle is shown in Figure 24. The injection total pressure and temperature ratios were set at 0.99 and 1.00. Both efficiencies decrease for increasing injection angle. This is due to the loss of the contribution of the injection flow to the streamwise momentum.

With pressure ratio set at 0.99, and injection angle at 30 degrees the effects of variations in the coolant total temperature were studied and the results are shown in Figure 24. Since heat transfer is not considered in the analysis, the temperature difference between the coolant and primary flow mainly affects the injection mass flow rate. As the temperature ratio decreases the injection velocity and mass flow decreases, so that the dependence of the performance parameters on injection mass flow may again be used to explain these results.

Finally, the blade pressure distribution for the design problem with and without injection are displayed in Figure 26. The injection pressure distribution differs only slightly from the no injection case, and separation was not indicated anywhere along the blade surface. These improvements in the injection pressure distribution from that of Figure 17 are due to the selection of injection row locations and the lower injection mass flows of the design problem.

Several observations may be made on the overall results of the study. First, although paired injection rows provide better film coverage, the two injection rows were found to interact with the main stream in such a way as to produce injection velocities in the downstream row which are twice those in the first row. Second a reduction in the coolant total temperature ratio from 1.00 to 0.50 resulted in reducing the injection mass flow from 8.5 to 6.6

percent for the coolant total pressure and injection angle under consideration. This fact has to be taken into consideration if the cold flow analysis is to be applied to a real problem. Third, if it can be avoided, injection should not occur before or at the throat of the cascade passage, since sonic velocities are likely to result. Last, for a given coolant flow condition, larger injection angles are more disruptive to the inviscid core flow.

CONCLUSIONS

The major findings of this analytical study are concerned with the aerodynamic performance of film cooled turbine cascades. Several film cooling configuration parameters were found which significantly effect cascade performance.

Injection from the suction side of the blade and particularly the aft portion of the suction surface towards the trailing edge produces the largest losses or worst performance. These losses are sometimes attributed to boundary layer separation, but the analytical injection induced separation model of this report shows the flow in the region to be fairly stable. Two possible causes for the suction side injection were analytically observed during the course of the study. First, high primary flow velocities are encountered along most of the suction surface, which increases the difference between injection and primary flow velocities. The larger energies consumed in accelerating the injection flow through this difference create the loss. Second, analytical calculations showed that the flow angle near the trailing edge plane was decreased by suction side injection. However, the calculated blade circulation varied only moderately, and the average downstream turning angle of the cascade was changed only slightly. Thus losses could be attributed to the energy used in returning the locally disturbed flow to the downstream angle dictated by the circulation.

For a given injection mass flow, pressure surface injection calculations generally gave performance numbers which indicated

lower losses than those for suction side injection at the same mass flow. This appears to be a consequence of the slower surface velocities which decreases the difference between injection and surface velocities and a continually favorable pressure gradient, which keeps boundary and film cooling layers thin. The analytical model did indicate that an injection induced separation bubble can occur on the pressure side if the injection row is located just aft of the blade leading edge where a pressure dip and recompression cause an unstable flow condition. Injection in this type of flow region should be avoided since a hot spot on the blade surface is likely developed at the separation.

As disruptive to the flow field as leading edge injection appeared in the analytical solutions, it produces surprisingly low losses. Reasons for not using leading edge injection are the development of large regions of stagnation flow on leading edge surface between injection rows which were indicated by the analytical model and the high internal blade pressures needed to produce a given injection velocity. Although trailing edge injection is of no use for film cooling, it was the one injection location found, which improves cascade performance by filling the viscous wake with higher energy injection fluid. Trailing edge injection is therefore the best means of internal cooling fluid discharge out of the blade.

When compared to location of injection, variation in injection angle appeared to have the second most significant effect on cascade losses. The closer the injection is to being perpendicular to the blade surface the larger the losses and the more likely separation is to occur. This is substantiated by the analytical solution of this report and the experimental work of others. In the transpiration cooling method, where perpendicular injection is employed, the injection velocity must be kept very low if the total injection mass flow, and cascade performance are to remain reasonable.

The least significant of the injection configuration parameters in the study was the injection row grouping. Pairing of injection rows so that ports may be staggered to provide better

film coverage did not excessively alter cascade performance. The combination of injection rows from different surface locations was found to produce additive performance characteristics. One important finding of the analytical study which had not been noted experimentally is the effect of mutual interaction between injection rows, which are closely grouped together. At the downstream row, a low pressure region is created by the upstream injection so that its velocity and mass flow can be several times the upstream row values in the low injection mass flow case. Alternately the stronger injection of the downstream row creates a higher inviscid pressure over the upstream row, reducing its injection velocity. The worst interaction effects resulted at the low injection mass flow rates, since the downstream injection can dominate the upstream row and induce such a high pressure that fluid is forced into the blade through the upstream row.

In addition to effects of the coolant injection on cascade performance, another finding of the analytical study was the interaction effects of the coolant injection on the primary flow. For the typical case of unseparated flow over a single row, the main flow acts as though the injection flow is a bump on the body surface. The flow decelerates as it approaches the column of injection fluid and accelerates as it moves over the injection row. The peak velocity is located just past the injection row. The larger the injection velocity the stronger this interaction. The analysis showed that separation does not generally occur with the injection mass flows used in turbine cooling and can usually be avoided by a good choice of injection sites. But if the flow does separate, the analytical solution indicates that the geometry of the blade passage or a downstream injection will normally terminate the separation region before it reaches the trailing edge. It was also shown that grouping of injection rows close together almost always results in separation between the rows. The final analytical observation on interaction effects is that primary flow reacts strongly to

injection located just before or at the blade passage throat. The injection at the throat often forces the main flow into trans- and supersonic flow regimes.

As one reviews the literature on film cooled turbines, four aerodynamic performance parameters are found to be used by most investigators. After using all these parameters in this study, a ranking of their usefulness may be made. Of the four, the thermodynamic efficiency is the best indicator of injection cascade performance. Primary air efficiency's chief merit is that it clearly indicates the effect of the coolant mass flow on performance. However, it often takes on values greater than one because of the ratio of the injection plus primary mass flow to primary mass flow used in its formulation. This may give the designer a false sense that he is getting more performance out of the injection process than exists in reality. Kinetic energy and pressure loss coefficients are the classical aerodynamic parameters, but they do not accurately represent the performance of a cascade with injection.

As a final observation or conclusion, it is noted that most studies correlate aerodynamic performance of film cooled blades with injection mass flow rate. This can be misleading to a designer since injection mass flow is dependent on the injection velocity and port area. It was found in this investigation that aerodynamic performance is more directly related to injection velocity than mass flow. The higher the injection velocity the larger the performance loss which is incurred.

After the finish of the work on this grant, a discrepancy was found. It was determined that the turbine cascade configuration analyzed in this report was not the same as that of reference [16]. The stagger angle of the cascade used here was less. If the correct stagger angle were used it would be found that the calculated aerodynamic performance curves for injections in the diffusion regions of the suction surface would be lower by approximately 0.003 than those shown in figures 19 and 20.

REFERENCES

1. Johnsen, I.A. and Bullock, R.O., ed., The Aerodynamic Design of Axial-Flow Compressors, NASA SP-36, 1965.
2. Glassman, A.J., ed., Turbine Design and Application, Vol. I, II, III, NASA SP-290, 1973.
3. Stewart, W.L., Analysis of Two-Dimensional Compressible Flow Loss Characteristics Downstream of Turbomachine Blade Rows in Terms of Basic Boundary Layer Characteristics. NACA TN 3515, 1955.
4. Prust, H.W., "Boundary-Layer Losses," Turbine Design and Analysis, Vol. 2, NASA SP 290, 1973, pp. 93-124.
5. Küppers, K.H., "Temperaturmessungen an Zwei Ruhenden Gasturinen-Schaufelprofilen mit Grenzschichtkühlung," DVL-St-Bericht Nr. 82, 1944.
6. Papel, S. and Trout, A.M., Experimental Investigation of Air Film-Cooling Applied to an Adiabatic Wall by Means of an Axially Discharging Slot, NASA TN D-9, 1959.
7. Seban, R.A., "Heat Transfer and Effectiveness for a Turbulent Boundary Layer with Tangential Fluid Injection," J. of Heat Transfer, Trans. ASME, Series C, Vol. 82, 1960, pp. 303-312.
8. Harnett, J.P., Birkebak, R.C. and Eckert, E.R.G., "Velocity Distributions, Temperature Distributions, Effectiveness, and Heat Transfer for Air Injected Through a Tangential Slot into a Turbulent Boundary Layer," J. of Heat Transfer, Trans. ASME, 1961, pp. 293-306.
9. Schlichting, H., Boundary-Layer Theory, Transl. Kestin, J., McGraw-Hill, New York, Sixth Ed., 1968.
10. Kays, W.M., Convective Heat and Mass Transfer, McGraw-Hill, New York, 1966.
11. High Temperature Turbines, NATO, AGARD-CP-73-71, 1971.
12. Shuets, I.T. and Dyban, E.P., Air Cooling of Gas Turbine Rotors, Transl. WP-AFB, Rept. No. AD 281-848, 1962.
13. Stabe, R.G. and Dengler, R.P., Experimental Investigation of Aerodynamic Performance of Cooled Turbine Vanes at Gas to Coolant Temperature Ratios Up to 2.75, NASA TMX-2733, Lewis Research Center, 1973.

14. Prust, H.W. and Bartlett, W.M., Cold-Air Study of the Effect on Turbine Stator Blade Aerodynamic Performance of Coolant Ejection From Various Trailing Edge Slot Geometries I - Experimental Results, NASA TMX-3000, Lewis Research Center, 1974

15. Moffat, T.P., Prust, H.W. and Bartlett, W.M., Two-Dimensional Cold-Air Cascade Study of a Film Cooled Turbine Stator Blade. I - Experimental Results of Pressure-Surface Film Cooling Tests. NASA TM X-3045, Lewis Research Center, 1974.

16. Prust, H.W., Two-Dimensional Cold-Air Cascade Study of a Film Cooled Turbine Stator Blade. II - Experimental Results of Full Film Cooling Tests. NASA TM X-3153, Lewis Research Center, 1975.

17. Hartzel, J.E., An Experimental Investigation of the Effects of Massive Film Cooling on the Aerodynamics of a Turbine Airfoil. Ph.D. Thesis, The Ohio State University, Columbus, Ohio, 1970.

18. Hiroki, T. and Katsumata, I., "Design and Experimental Studies of Turbine Cooling," ASME Paper No. 74-GT-30, 1974.

19. Lokai, V.I. and Kumirov, B.A., "Experimental Study of Turbine Stage with Cooling Air Discharge into Flow Passage," Izvestiya Vuz. Aviatsionnaya Teknika. Vol. 13, No. 4, 1970, pp. 93-100.

20. Prust, H.W., An Analytical Study of the Effect of Coolant Flow Variables on the Kinetic Energy Output of a Cooled Turbine Blade Row. NASA TM X-67960, Lewis Research Center, 1972, AIAA Paper No. 72-12, 1972.

21. Hartzel, J.E., "Prediction of Effects of Mass-Transfer Cooling on the Blade Row Efficiency of Turbine Airfoils," AIAA Paper No. 72-11, 1972.

22. Tabakoff, W. and Hamed, A., "Theoretical and Experimental Study of Flow Through Turbine Cascades with Coolant Flow Injection," AIAA Paper No. 75-843, 1975.

23. Pavri, R. and Tabakoff, W., "An Analytical Solution of Wall-Temperature Distribution for Transpiration and Local Mass Injection over a Flat Plate," ASME Paper No. 72-HT-57, 1972.

24. Nilson, R.H. and Tsuei, Y.G., "Film Cooling by Oblique Slot Injection in High-Speed Laminar Flow," AIAA Journal, Vol. 13, No. 9, 1975, pp. 1199-1202.
25. Inger, G.R., "Laminar Boundary Layer Solutions with Strong Blowing," AIAA Journal, Vol. 5, No. 9, 1967, pp. 1677-1678.
26. Inger, G.R., "A Simple Model Shear Flow with Massive Blowing," AIAA Journal, Vol. 4, 1966, pp. 1834-1835.
27. Bergeles, G., Gosman, A.D. and Launder, B.E., "The Prediction of Three-Dimensional Discrete-Hole Cooling Processes: I - Laminar Flow," ASME Paper No. 75-WA/HT-109, 1975.
28. Sherman, A., Yeh, H., McAssey, E. and Reshotko, E., "Multiple Slot Laminar Film Cooling," AIAA Journal, Vol. 11, 1973, pp. 1413-1414.
29. Herring, H.J., "A Method of Predicting the Behavior of a Turbulent Boundary Layer with Discrete Transpiration Jets," ASME Paper No. 74-GT-48, 1974.
30. Aerodynamic Loss Analysis for Quasi-Transpiration Cooled Turbine Blades - Final Report. EDR 7796, Detroit Diesel Allison, Indianapolis, Indiana, 1973.
31. Goldstein, R.J., "Film Cooling," Advances in Heat Transfer, Vol. 7, Academic Press, New York, 1971, pp. 321-379.
32. Eckert, E.R.G., "Film Cooling with Injection Through Holes," High Temperature Turbines, AGARD CP-73-71, 1971.
33. Goldstein, R.J., Eckert, E.R.G. and Ramsey, J.W., "Film Cooling Following Injection Through Holes," J. of Engineering for Power, 1968, p. 385.
34. Metzger, D.E., Takeuchi, D.I. and Kuenstler, P.A., "Effectiveness and Heat Transfer with Full Coverage Film Cooling," J. of Engineering for Power, Vol. 95, 1973, pp. 180-184.
35. Metzger, D.E., Biddle, J.R. and Warren, J.M., "Evaluation of Film Cooling Performance on Gas Turbine Surfaces," High Temperature Turbines, AGARD CP-73-71, 1971.
36. Liess, C. and Carnel, J., "Application of Film Cooling to Gas - Turbine Blades," High Temperature Turbines, AGARD CP-73-71, 1971.

37. Bergeles, G., Gosmann, A.D. and Launder, B.E., "The Near-Field Character of a Jet Discharged Through a Wall at 90 Deg. to a Main Stream," ASME Paper No. 75-WA/HT-108, 1975.

38. Crawford, M.E., Kays, W.M. and Moffat, R.J., "Heat Transfer with Full-Coverage Film Cooling Using 30-Deg. Slant-Angle Injection," ASME Paper No. 75-WA/HT-11, 1975.

39. Crawford, M.E., Choe, H., Kays, W.M. and Moffat, R.J., "Full Coverage Film Cooling Heat Transfer Study - Summary of Data for Normal-Hole and 30° Slant-Hole Injection," NASA CR-2648, 1976.

40. Brown, A. and Minty, A.G., "The Effects of Mainstream Turbulence Intensity and Presure Gradient on Film Cooling Effectiveness for Cold Air Injection Slits of Various Aspect Ratios," ASME Paper No. 75-WA/HT-17, 1975.

41. Odgers, J. and Son, N.N., "Film Cooling - The Effect of a Cold Jet Normal to the Coolant Layer," ASME Paper No. 75-WA/GT-4 1975.

42. Hess, J.L., "Review of Integral-Equation Techniques for Solving Potential-Flow Problems with Emphasis on the Surface-Source Method," Computer Methods in Applied Mechanics and Engineering, Vol. 5, No. 2, 1975, pp. 146-196.

43. Martensen, E., The Calculation of the Pressure Distribution on a Cascade of Thick Airfoils by Means of Fredholm Integral Equations of the Second Kind. Transl., NASA TT F-702, 1971.

44. Hess, J.L. and Smith, A.M.O., "Calculation of Potential Flows About Arbitrary Bodies," Progress in Aeronautical Sciences, Vol. 8, Pergamon Press, New York, 1966.

45. Geller, W., "Incompressible Flow Through Cascades with Separation," Boundary Layer Effects-in Turbomachinery, AGARD-ograph, 1972, pp. 171-186.

46. Van Den Braembussche, R.A., "Calculation of Compressible Subsonic Flow in Cascades with Varying Blade Height," J. of Engineering for Power, Vol. 95, No. 4, 1973, pp. 345-351.

47. Hess, J.L., "Higher Order Numerical Solution of the Integral Equation for the Two-Dimensional Neumann Problem," Computer Methods in Applied Mechanics and Engineering. Vol. 2, 1973, pp. 1-15.

48. Geising, J.P., Extension of the Douglas Neuman Program to Problems of Lifting Infinite Cascades, Douglas Report No. LB-31653, Government Report No. AD-605207, 1964.

49. Geising, J.P. and Smith, A.M.O., Potential Flow About Two-Dimensional Hydrofoils," J. of Fluid Mechanics, Vol. 28, 1967, pp. 113-129.

50. Bristow, D.R., "A New Surface Singularity Method for Multi-Element Airfoil Analysis and Design," AIAA Paper No. 76-20, 1976.

51. Dilley, A.D., Integral Equation Solution Technique for Two-Dimensional Potential Flow Problems, M.S. Thesis University of Cincinnati, Cincinnati, Ohio, 1976.

52. Stevens, W.A., Goradia, S.H. and Braden, J.A., Mathematical Model for Two-Dimensional Multi-Component Airfoils in Viscous Flow, NASA CR-1843, 1971.

53. Gostelow, J.P., "Trailing Edge Flows Over Turbomachine Blades and the Kutta-Joukowsky Condition," ASME 75-GT-94, 1975.

54. Gostelow, J.P., Potential Flow Through Cascades Extensions to an Exact Theory, A.R.C. CP No. 808, 1964.

55. Geller, W., "Calculation of the Turning Angle of Two-Dimensional Incompressible Cascade Flow," AIAA Journal, Vol. 14, No. 3, 1976, pp. 297-298.

56. McDonel, J.D., Cascade Loss Prediction, M.S. Thesis, University of Cincinnati, Cincinnati, Ohio 1969.

57. Gostelow, J.P., Lewkowicz, A.K. and Shaalan, M.R.A., Viscosity Effects on the Two Dimensional Flow in Cascades, A.R.C. CP No. 872, 1965.

58. Davis, R.T. and Werle, M.J., "Numerical Methods for Interacting Boundary Layers," Proceedings of 1976 Heat Transfer and Fluid Mechanics Institute, Stanford University Press, Stanford, 1976, pp. 317-339.

59. Stewartson, K., "Multistructured Boundary Layers on Flat Plates and Related Bodies," Advances in Applied Mechanics, Vol. 14, Academic Press, Inc., 1974, pp. 145-239.

60. Shapiro, A.H., The Dynamics and Thermodynamics of Compressible Fluid Flow, Vol. I, Ronald Press Co., New York, 1953.

61. Stratford, B.S. and Beaver, G.S., The Calculation of the Compressible Turbulent Boundary Layer in an Arbitrary Pressure Gradient - A Correlation of Certain Previous Methods, A.R.C. R&M No. 3207, 1959.

62. Gostelow, J.P., Potential Flow Through Cascades - A Comparison Between Exact and Approximate Solutions, A.R.C. CP No. 807, 1963.

63. Herrig, L.J., Emery, J.C. and Erwin, J.R., Systematic Two-Dimensional Cascade of NACA 65-Series Compressor Blades at Low Speeds, NACA TN-3916, 1957.

64. Whitney, W.J., Szanca, E.M., Moffitt, T.P., and Monroe, D.E., Cold-Air Investigation of a Turbine for High-Temperature Engine Applications, NASA TN-D-3751, 1967.

65. McFarland, E.R., An Investigation of the Aerodynamics Performance of Film Cooled Turbine Blades, Ph.D. Thesis, University of Cincinnati, Cincinnati, Ohio, 1976.

66. Prust, H.W., Two-Dimensional Cascade Study of a Film-Cooled Turbine Stator Blade. IV - Experimental Versus Analytical Results for Stator Blade With 12 Rows of 0.076 cm (0.030 in.) Coolant Holes, NASA TMX Lewis Research Center, to be published 1977.

LIST OF SYMBOLS

English Symbols

A	area
A_s, A_v	source-sink and vortex singularity influence coefficients for tangential or real velocity component at a point
$a+bi$	a general complex number or location in the complex plane
B_s, B_v	source-sink and vortex singularity influence coefficients for normal or imaginary velocity component at a point
C	complex potential function
c	location of singularity distribution
C_D	discharge coefficient for injection row
$C_{k\ell}$	combined defining matrix for use in relating the source-sink distribution to vortex distribution
C_p	coefficient of pressure
c_p	specific heat at constant pressure
c_1, c_2	end points of the line segment over which the singularities are distributed
D	coefficient matrix of the minimization equations
$\bar{e}$	kinetic energy loss coefficient
F	specified boundary condition function along the cascade body
$f(x)$	general real function
$f(z)$	general complex function
G	singularity strength density function
g	vortex singularity strength distribution
H_t	total enthalpy

h	distance along the imaginary reference axis to the intersection point of the imaginary axis and an extension of singularity line segment
i	the imaginary number, $\sqrt{-1}$
K	combined concentrated singularity strength of the cascade body as seen from the far stream boundary conditions
k	combined singularity strength distribution, $(s+ig)$
ℓ	length of the sides of the polyhedron used to approximate the cascade body
M	Mach number
M_{CR}	critical velocity ratio
n	number of sides in the approximating polyhedron
$\bar{n}_t$	unit outward normal vector to cascade body
P	static pressure
P_t	total pressure
P_o	static pressure at the outer boundary of the mixing layer
Q	constrained singularity strength density function for minimization
q	dynamic pressure
$\bar{R}$	radial vector from cascade
R	gas constant for ideal gas equation
r	radius or distance from a point in any direction
S	cascade spacing
s	source-sink singularity strength distribution
T	static temperature
T_t	total temperature
t	streamwise coordinate along the cascade body, also trailing edge thickness

V	general velocity
v	disturbance velocity due to the cascade
W	weight or mass flow rate, also complex velocity due to a surface singularity
w	complex velocity due to a singularity distribution
x	real coordinate axis of the reference coordinate system
$x+iy$	general location in the reference complex plane
y	imaginary coordinate axis of the reference coordinate system
z	general complex number or location in the reference complex plane

Greek Symbols

α	flow angle, also orientation angle of singularity line element
β	cascade stagger angle
β_k	onset flow contribution to the relation between source-sink distribution and vortex distribution
Γ	concentrated vortex strength of the cascade body as seen from the far stream boundary condition
Γ_{cir}	circulation about cascade body
γ	ratio of specific heats
Δ	finite incremental change in a variable
δ	boundary layer displacement thickness
Δ_s, Δ_v	areas of influence of the source-sink and vortex singularities
$\Delta\theta$	turning angle of the cascade flow
η	orientation angle of singularity line element
η_{PA}	primary air efficiency
η_{TH}	thermodynamic efficiency

θ	injection flow angle to cascade body surface, orientation angle of the singularity line element and boundary layer momentum thickness
λ	compressible flow correction factor
$\lambda_1\lambda_1$	Lagrangian multipliers of the constraints in the minimization equations
ξ	ratio of coolant flow to primary or mixing layer flow, also coordinate line along the singularity line element
ρ	static density
ρ_t	total density
Σ	concentrated source-sink strength of the cascade body as seen from the far stream boundary conditions
σ	cascade solidity
ϕ	velocity potential
ψ	stream function
ω	pressure loss coefficient

Other Symbols

∇	gradient vector operator
$(\bar{})$	vector quantity
Re( )	real portion of complex variable
Im( )	imaginary portion of complex variable
$[\ ]_{\ell xk}$	matrix with ℓ rows and k columns

Subscripts

BODY	evaluated along the cascade body surface
c	coolant or injection flow quantity
comp	compressible flow corrected variable
cr	gas dynamic critical condition
E,2	far downstream station or exit flow condition
I	far upstream station or inlet flow condition

i,j,k,ℓ,m	matrix and equation indices
inv	inviscid flow variables
inc	incompressible flow variable, also incidence angle
m	mixed flow condition downstream of an injection row in the mixing layer
N,T	normal and tangential components of velocity and forces at points on the cascade body surface or anywhere in the flow field
onset	variables which are defined as constant throughout the flow field
sep	quantities which are associated with the injection induced separation model
t	physical state variables which are evaluated at total conditions, also components of variables evaluated along the body surface
TE	quantities associated with the trailing edge of the cascade body
u	flow conditions in the upstream or unmixed region of the mixing layer before flow has crossed the injection row
x,y	components of variables which are aligned with the reference coordinate system
z	quantity evaluated at any general point in the flow field
∞	quantities evaluated at stations far removed from the cascade row

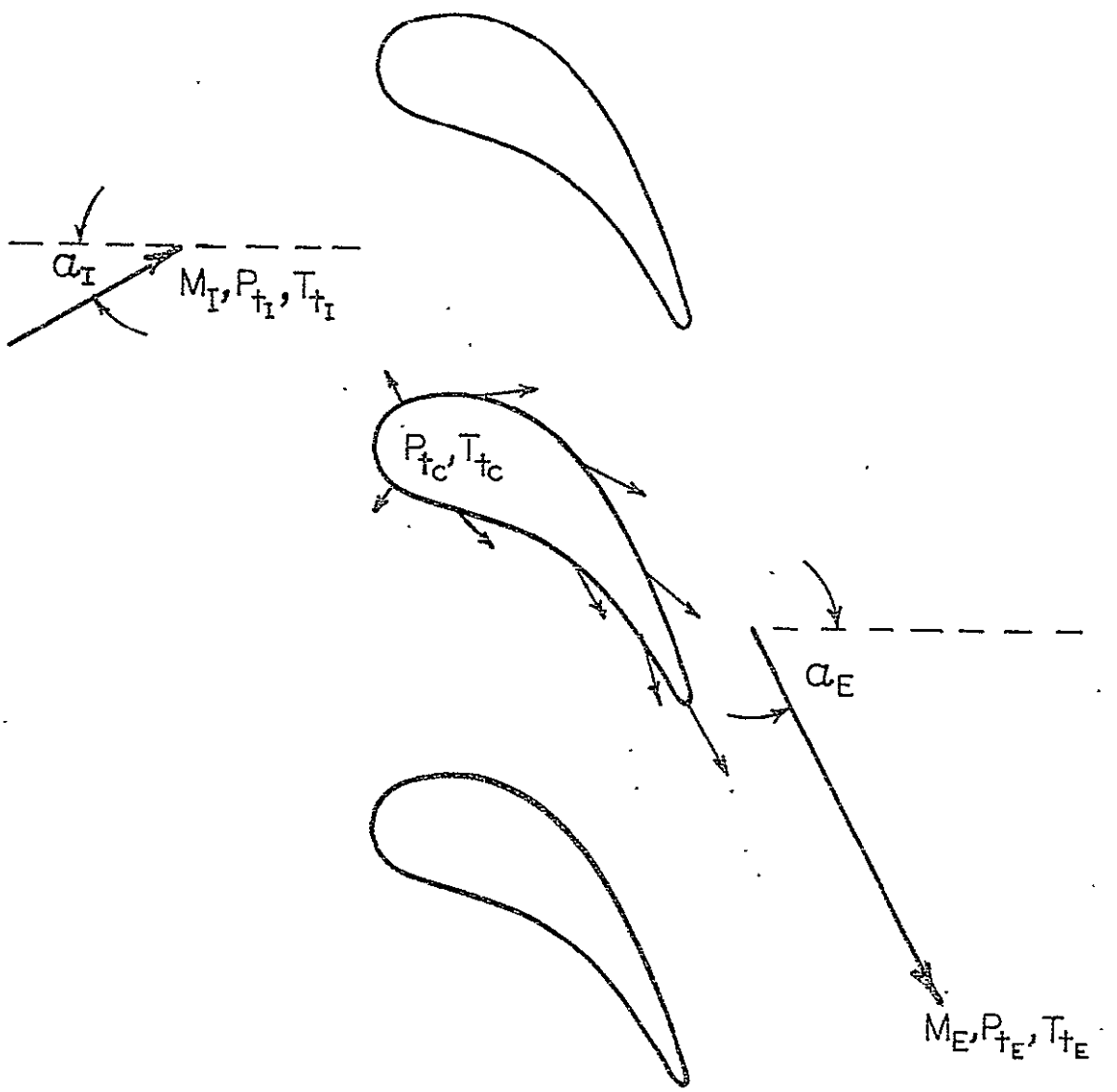

FIGURE I. MODEL PROBLEM

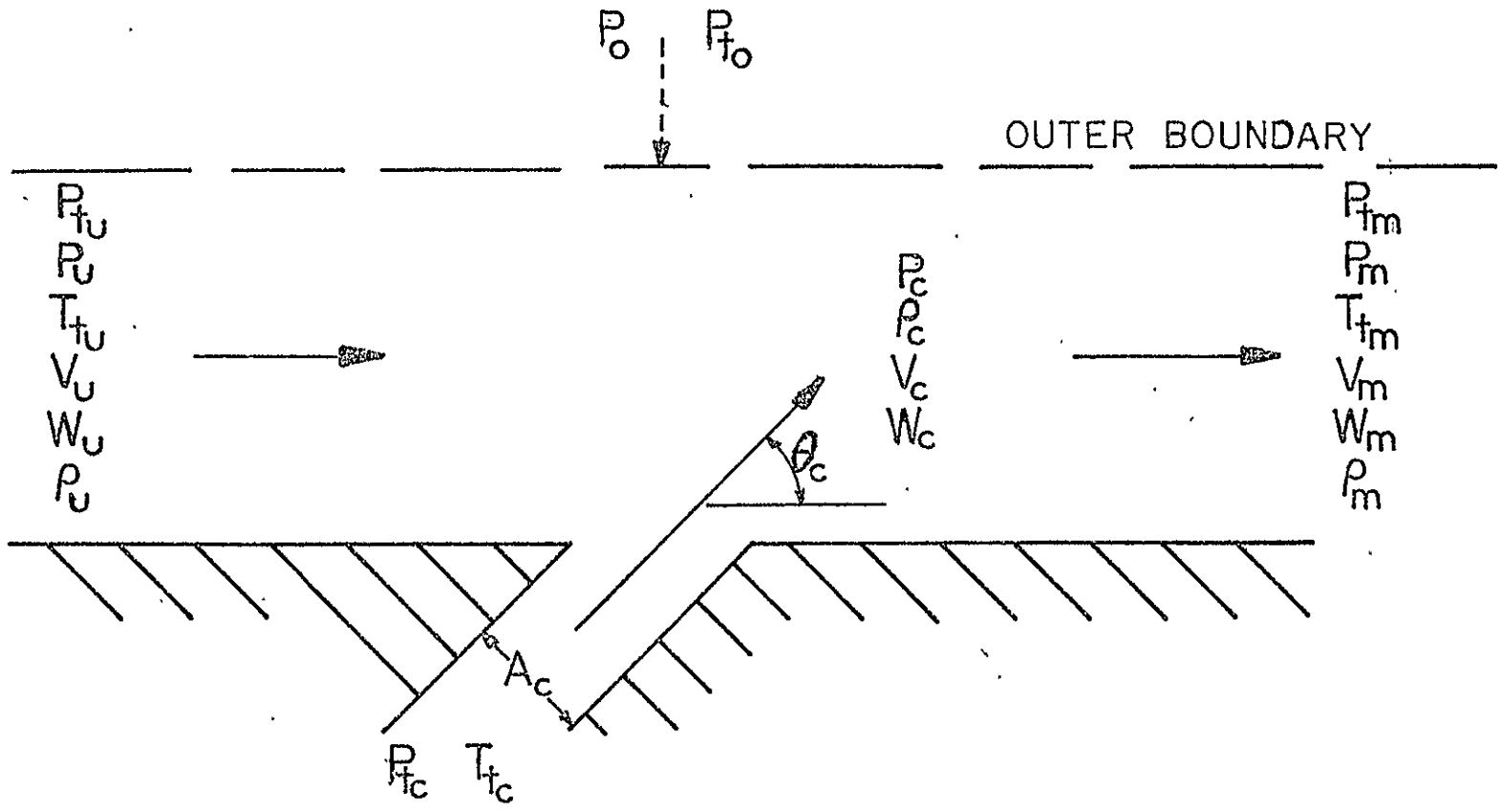

FIGURE 2. ONE DIMENSIONAL MIXING MODEL

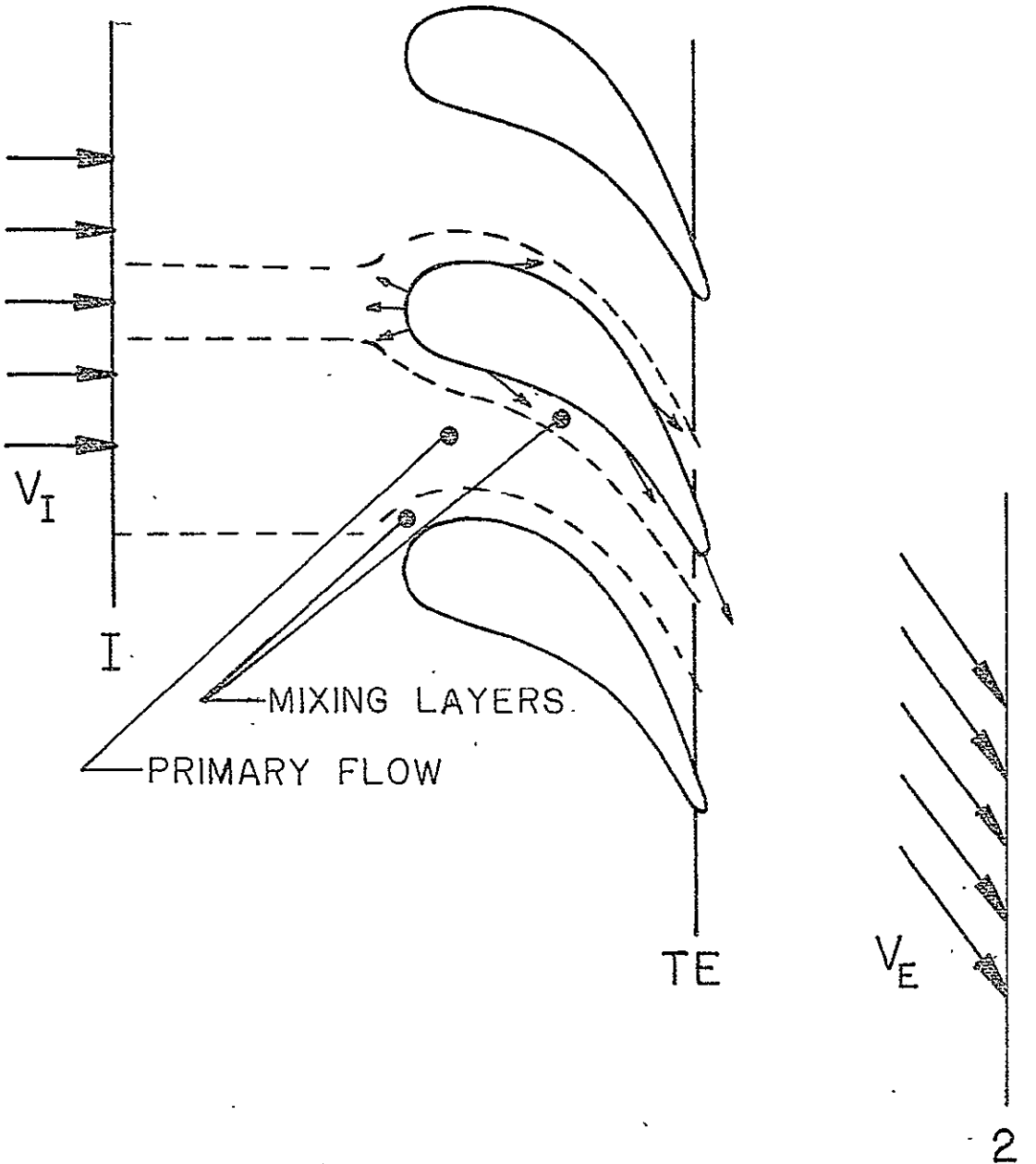

FIGURE 3. COMPOSITE MIXING METHOD

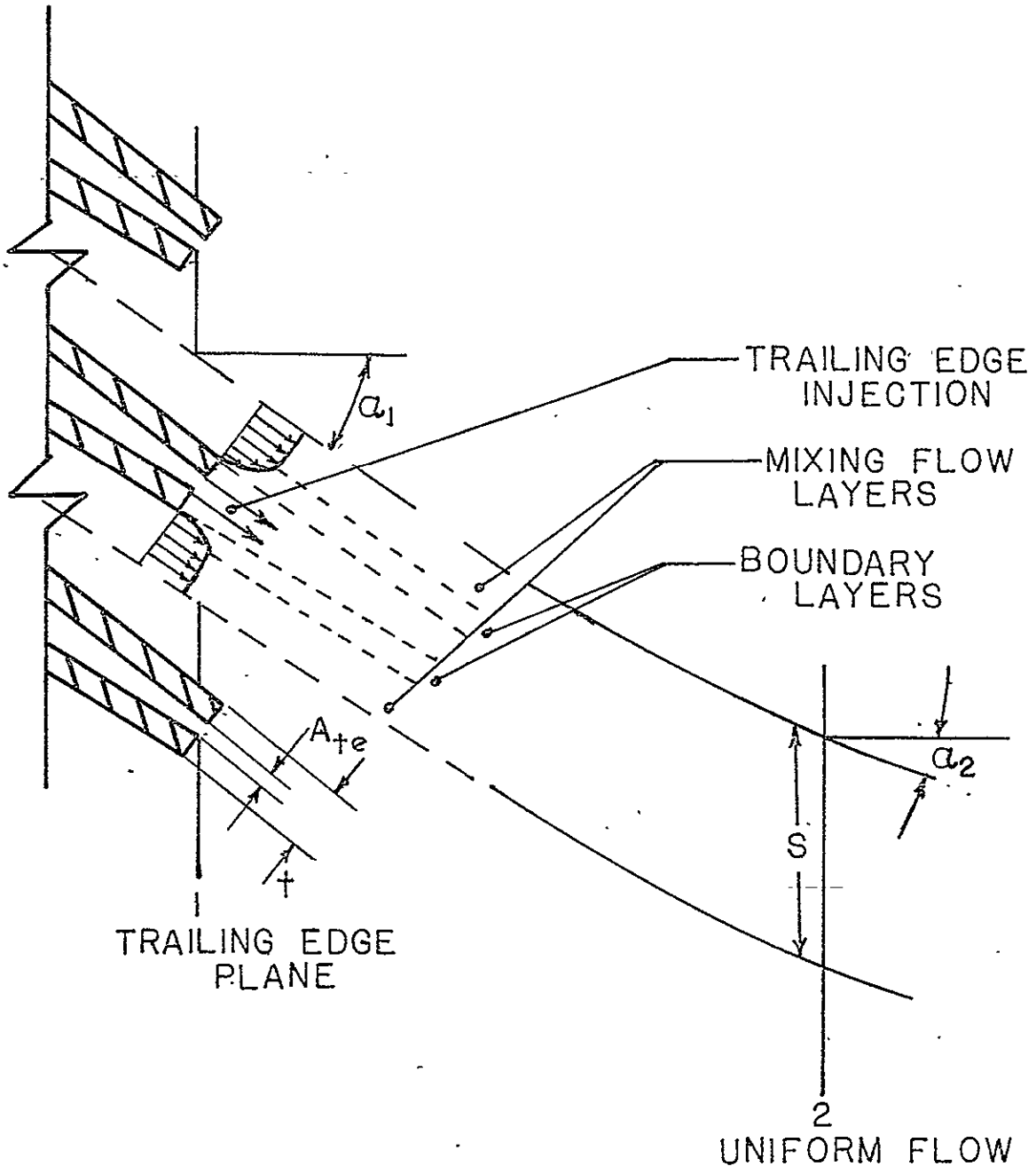

FIGURE 4. CASCADE LOSSES WITH INJECTION

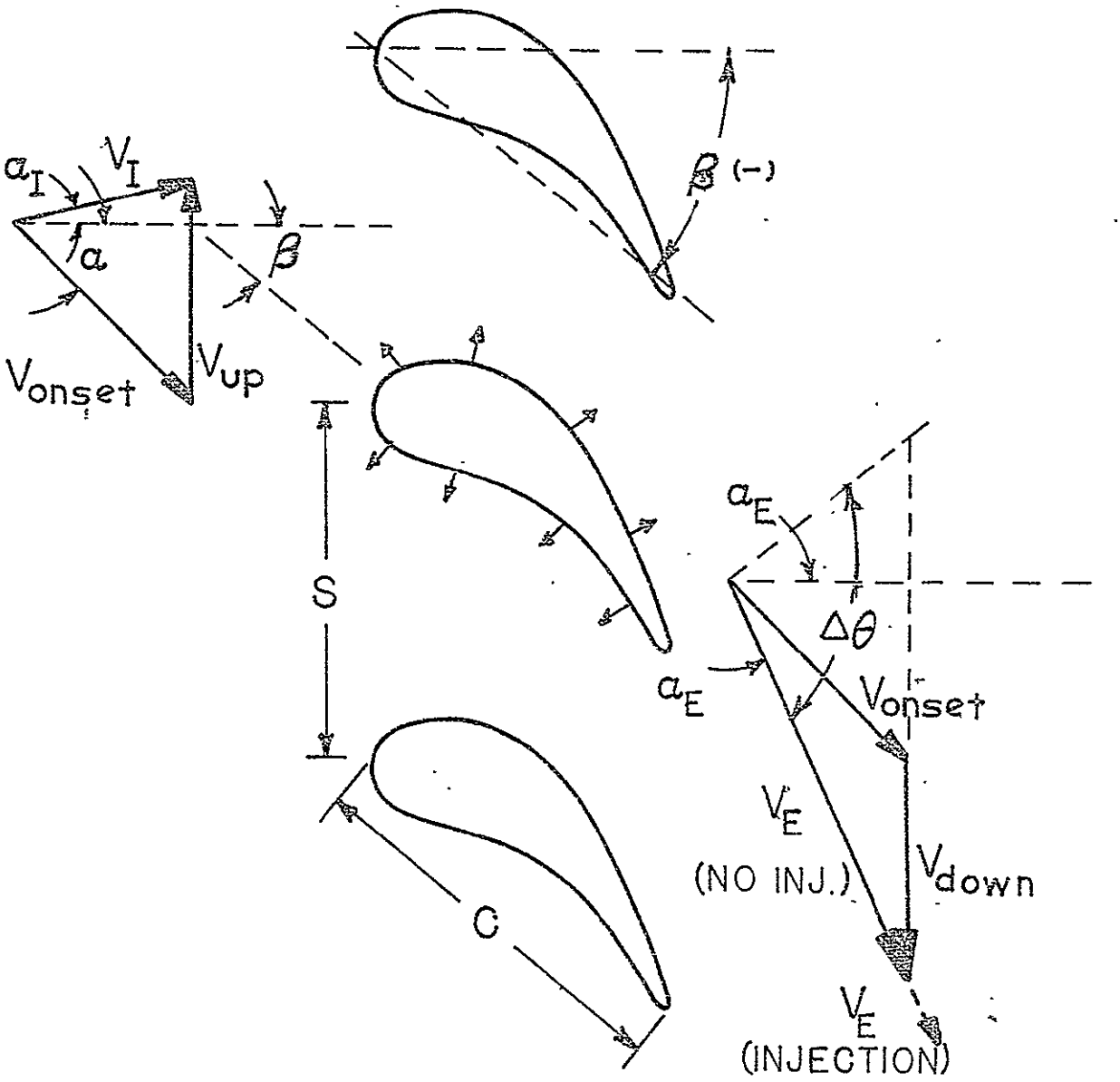

FIGURE 5. INVISCID CASCADE PROBLEM

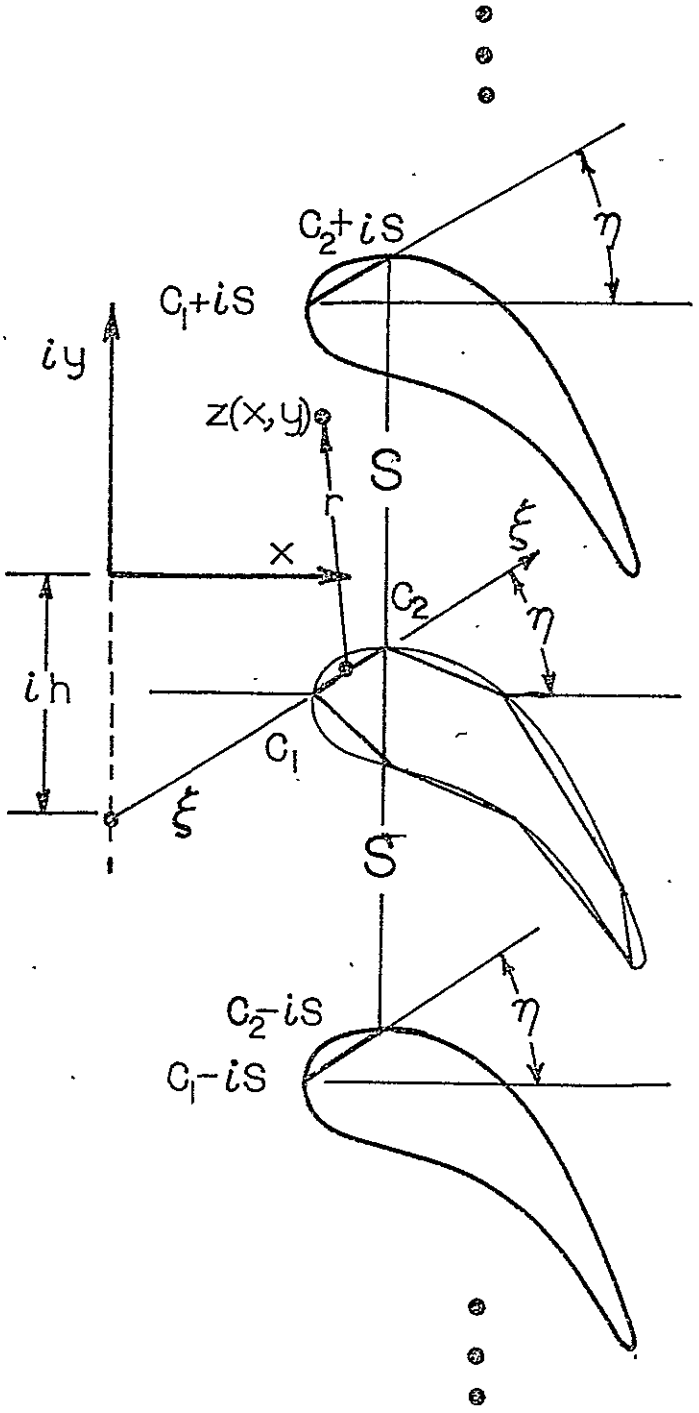

FIGURE 6. SINGULARITY DISTRIBUTION GEOMETRY

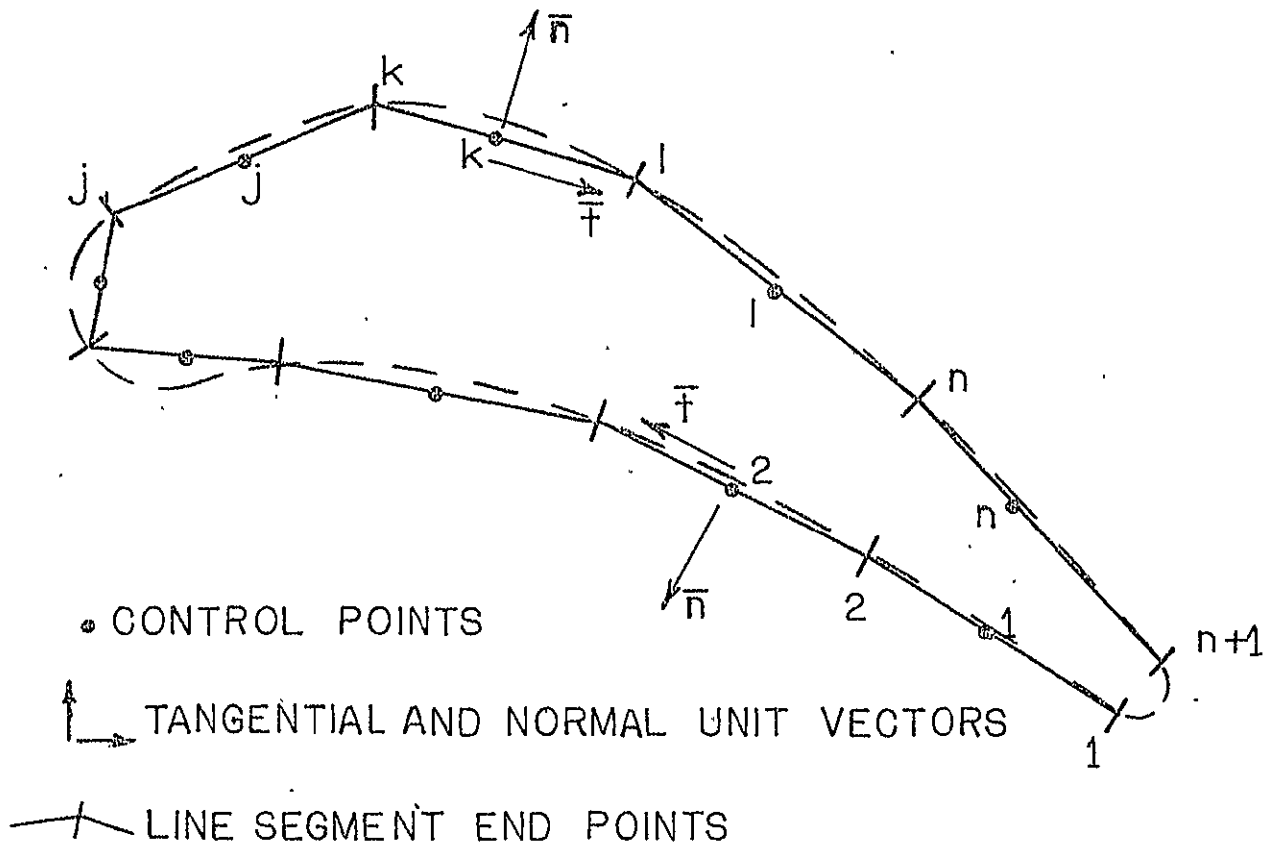

FIGURE 7. POLYHEDRON APPROXIMATION OF BLADE

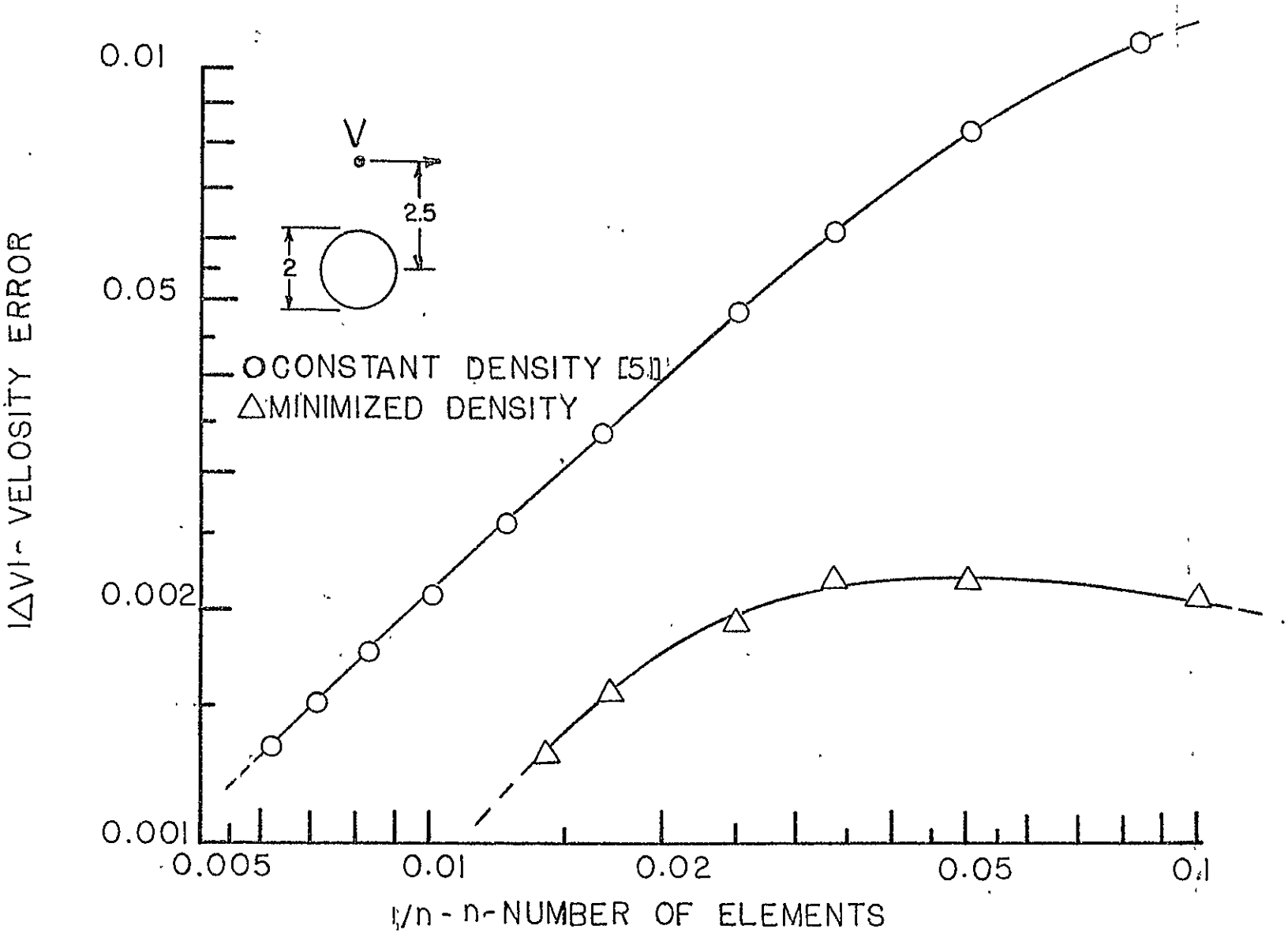

FIGURE 8. ACCURACY STUDY - SINGLE BODY

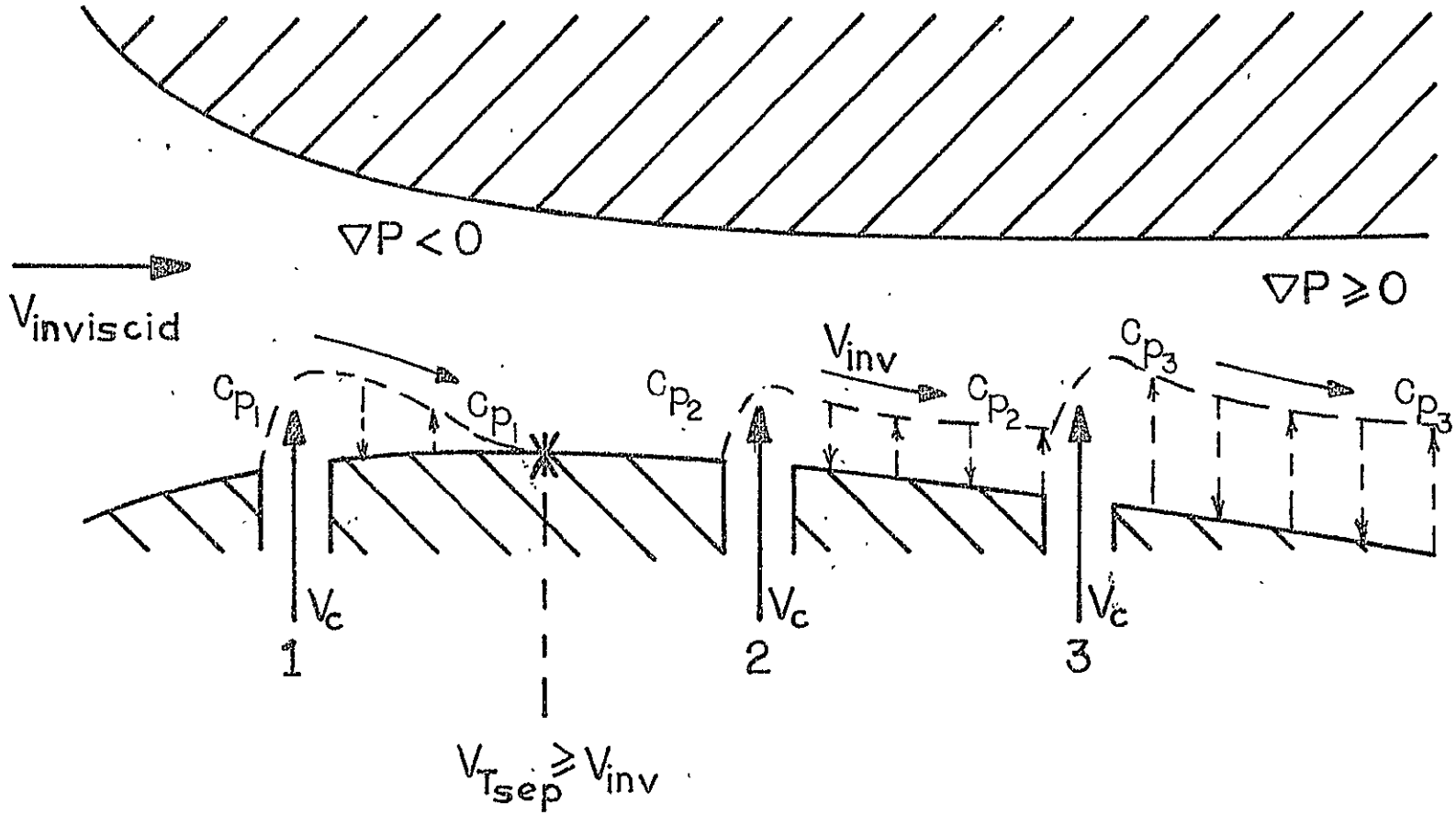

FIGURE 9. SEPARATION MODEL

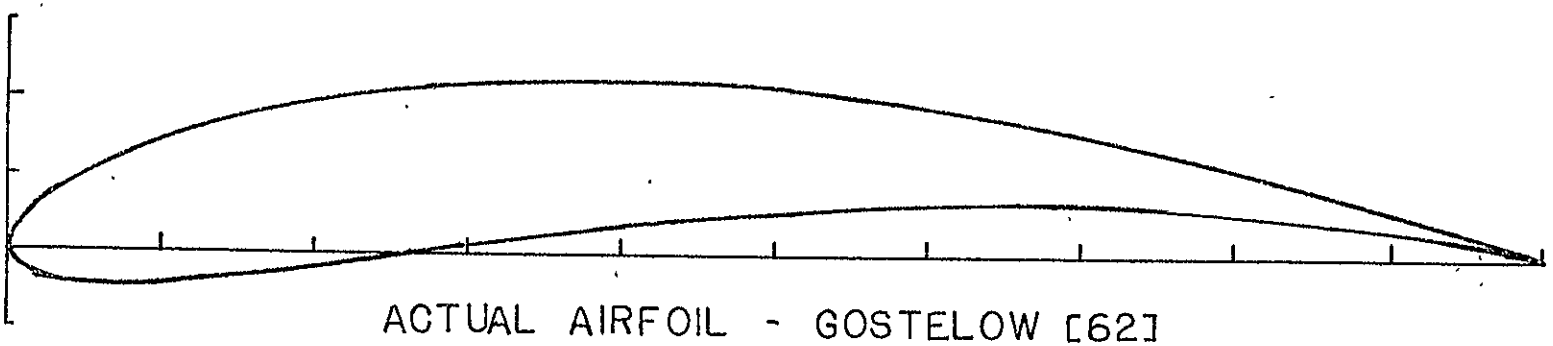

ACTUAL AIRFOIL - GOSTELOW [62]

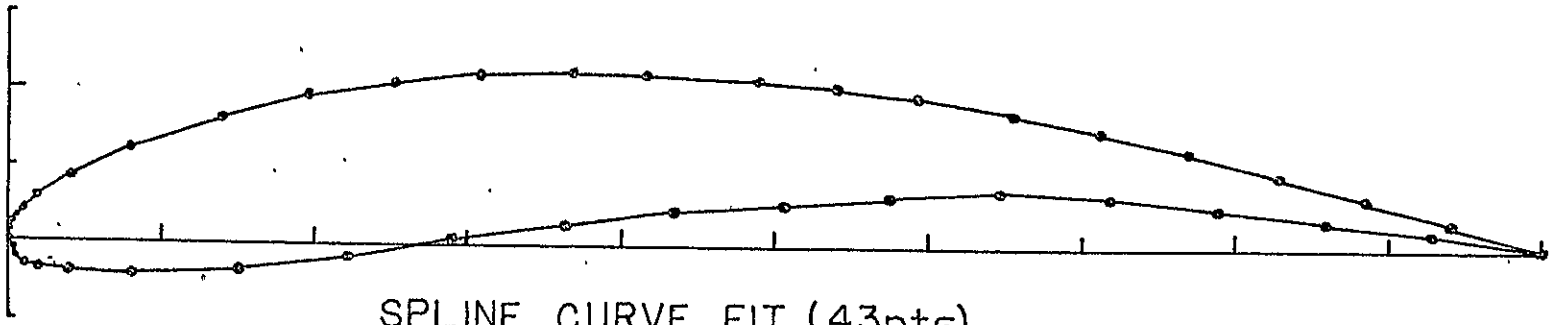

SPLINE CURVE FIT (43pts)

FIGURE 10. EXACT SOLUTION AIRFOIL

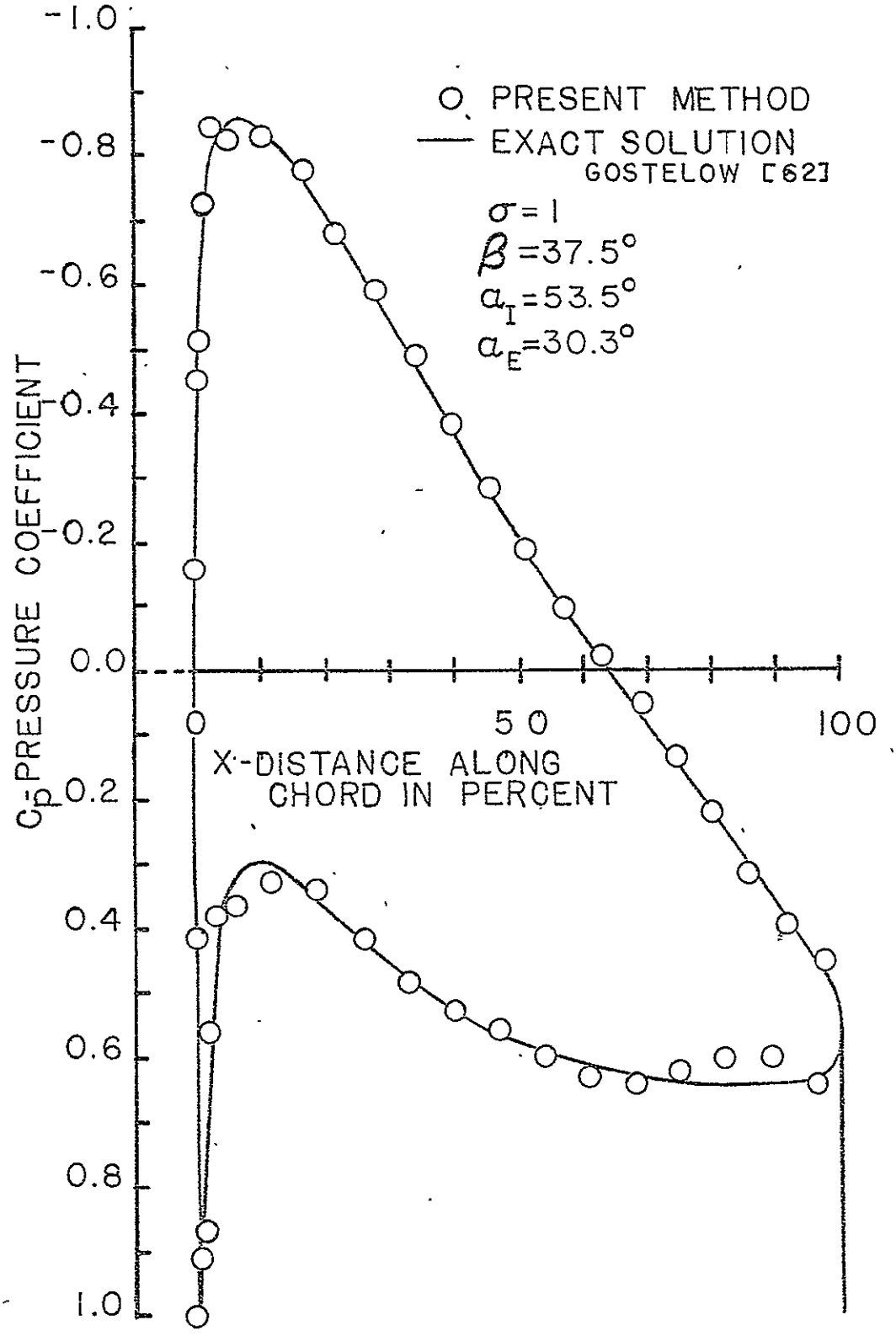

FIGURE 11. COMPARISON WITH EXACT SOLUTION - POTENTIAL FLOW

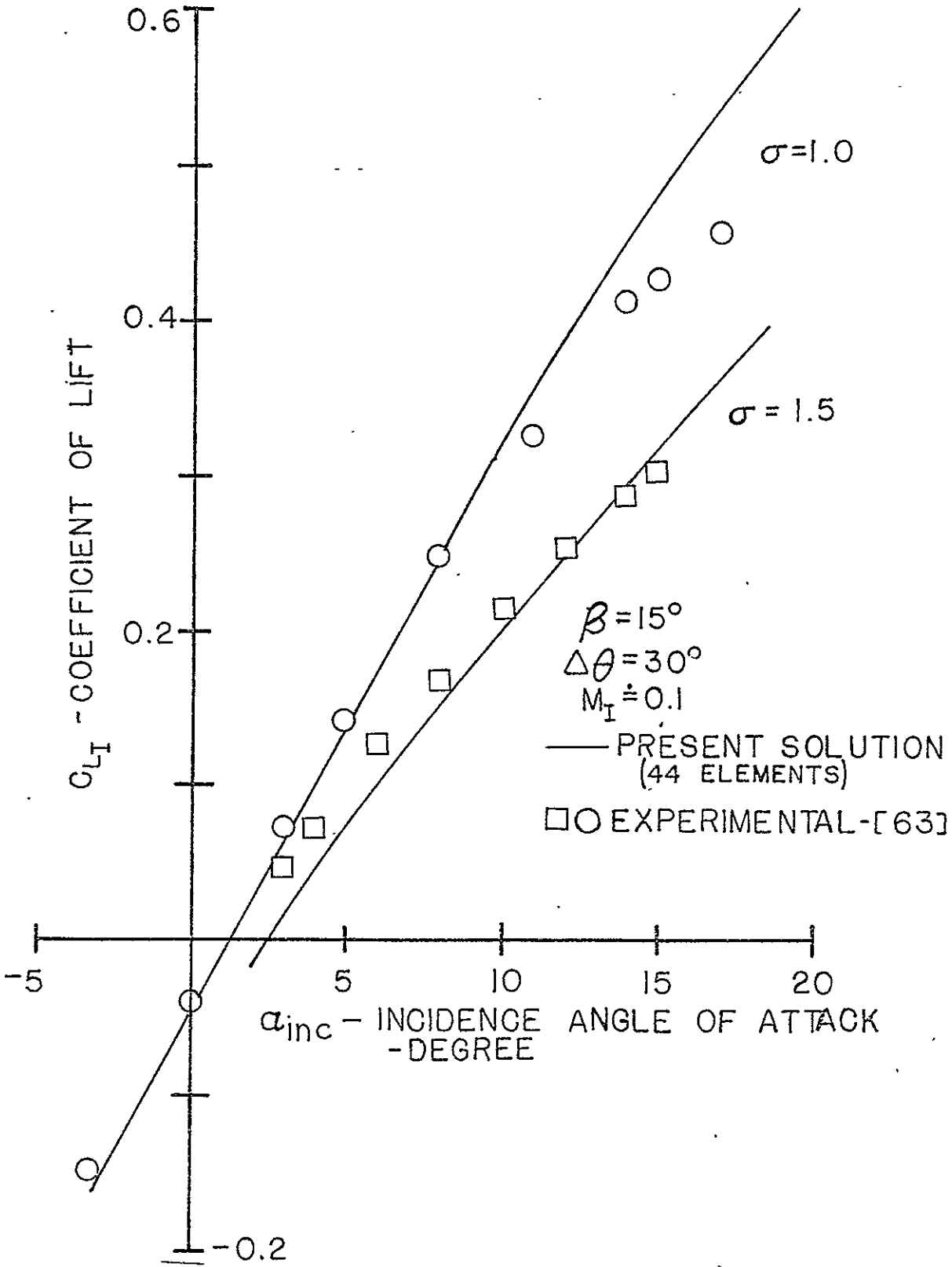

FIGURE 12. LIFT CURVE FOR CASCADE OF SYMMETRIC AIRFOILS

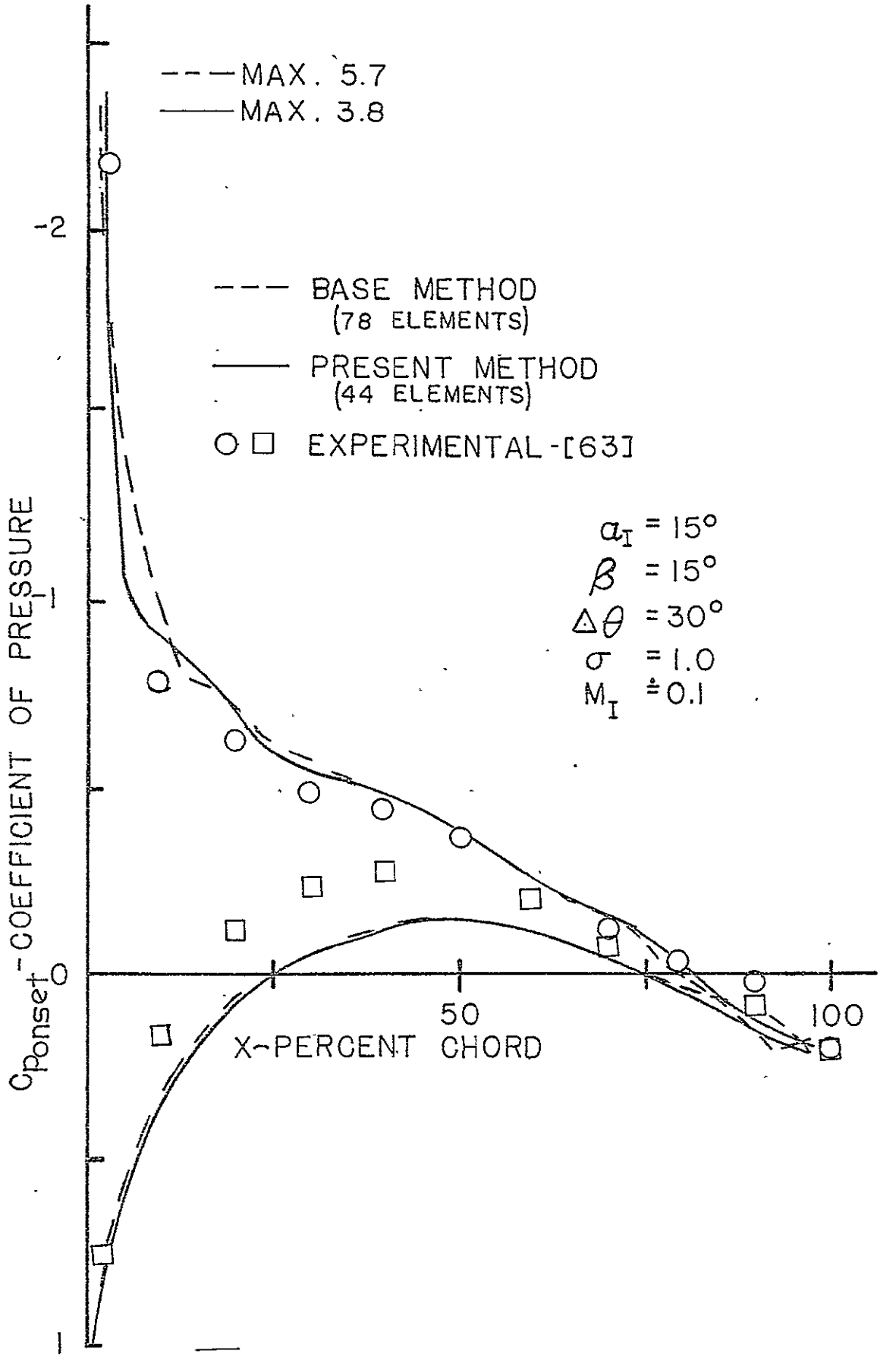

FIGURE 13. PRESSURE DISTRIBUTION FOR CASCADE OF SYMMTRIC AIRFOILS

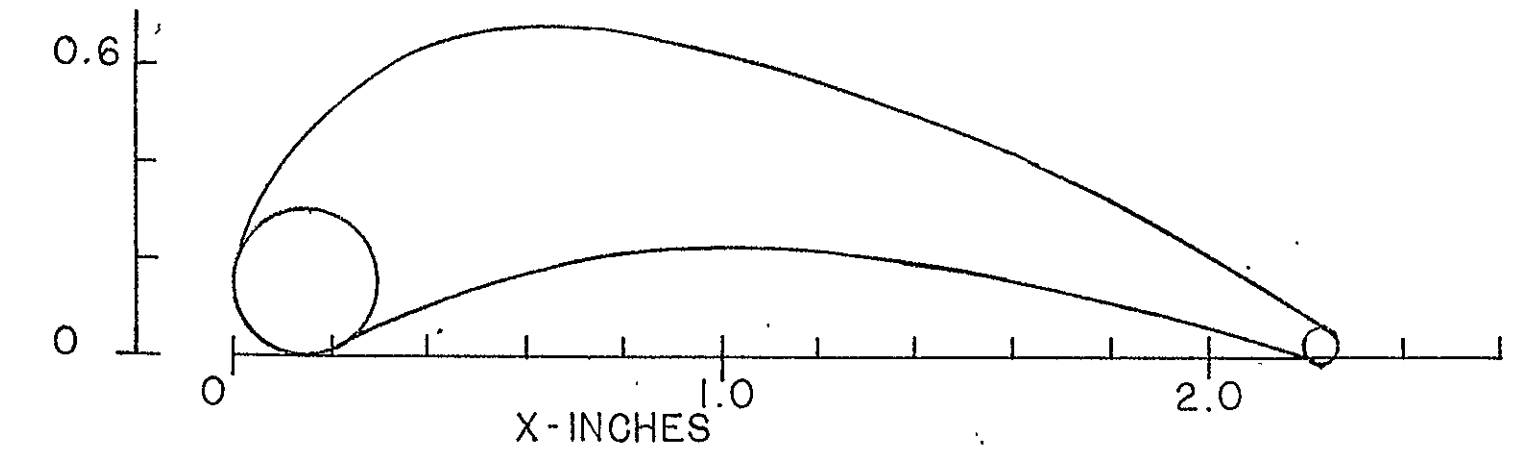

ACTUAL TURBINE BLADE-WHITNEY[64],RRUST[16]

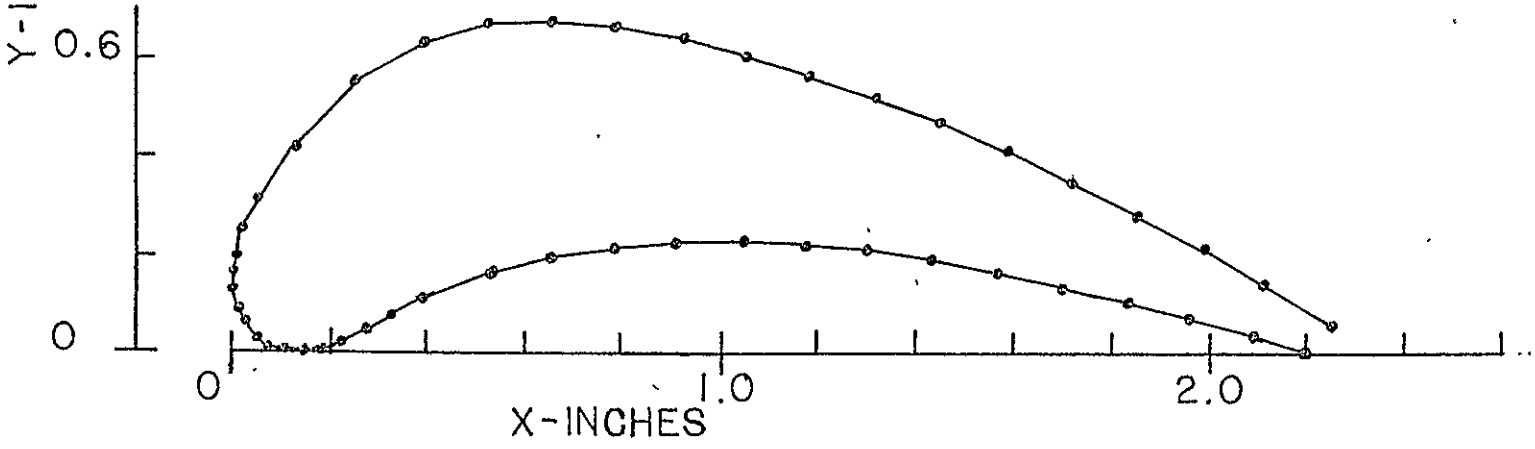

SPLINE CURVE FIT BLADE-47 POINTS

FIGURE 14 COMPRESSIBLE SOLUTION - TURBINE BLADE

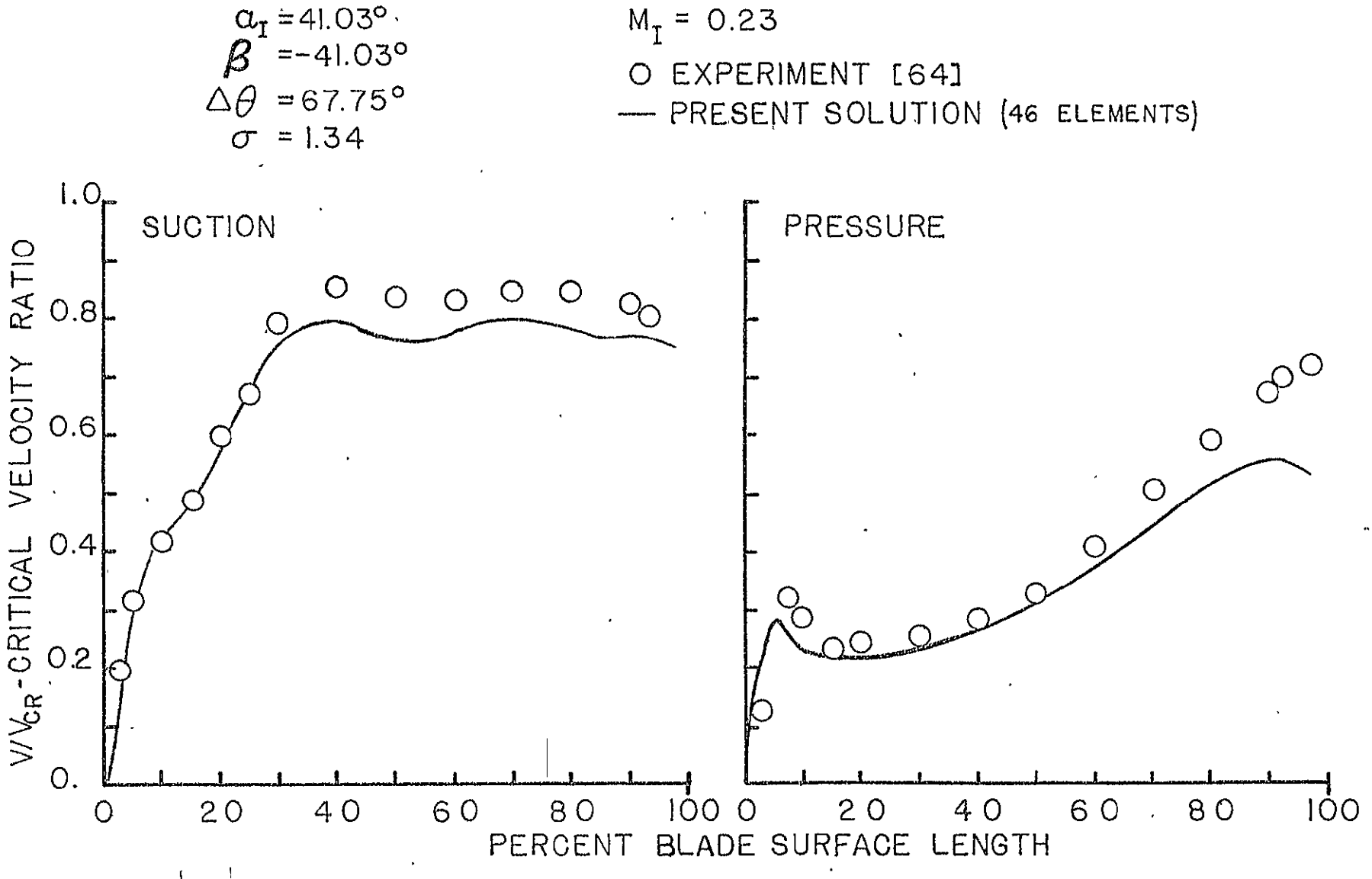

FIGURE 15 TURBINE BLADE SOLUTION - COMPRESSIBLE FLOW

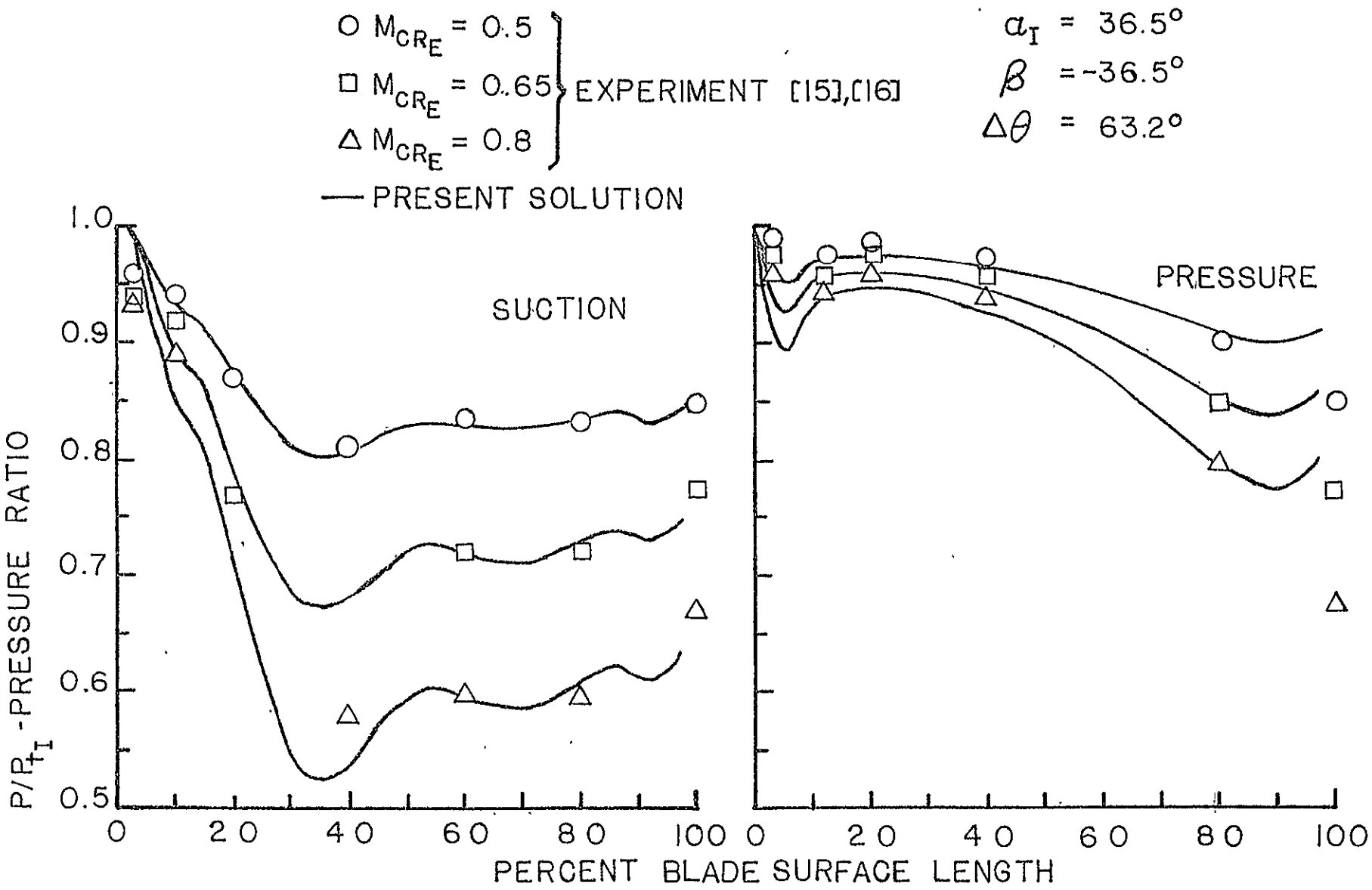

FIGURE 16. PRESSURE DISTRIBUTION - COMPRESSIBLE FLOW

$a_I = 36.5°$ $\sigma = 1.34$

$\beta = -36.5°$ CONFIGURATION - PRUST [16]

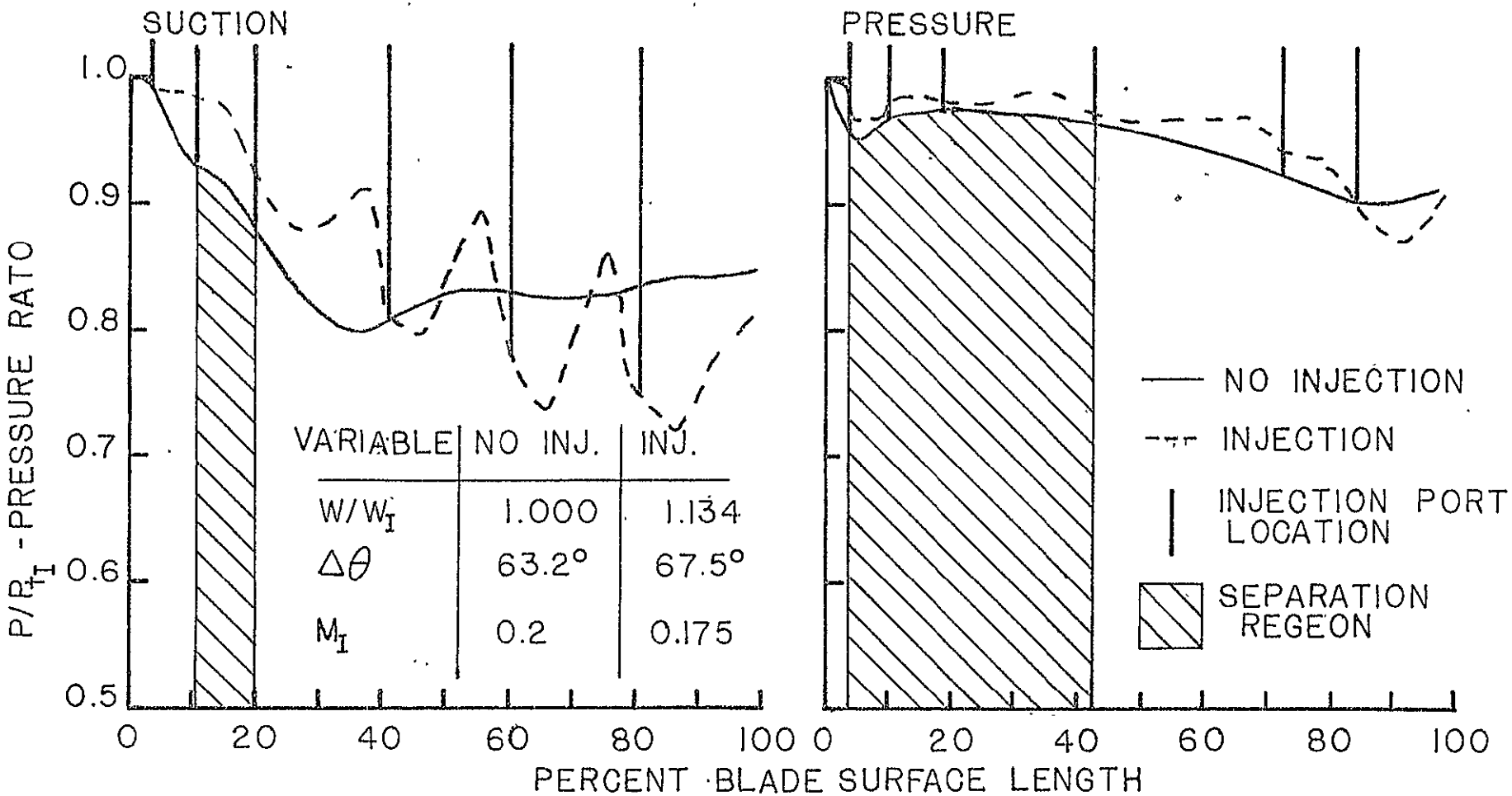

FIGURE 17: PRESSURE DISTRIBUTION WITH AND WITHOUT INJECTION

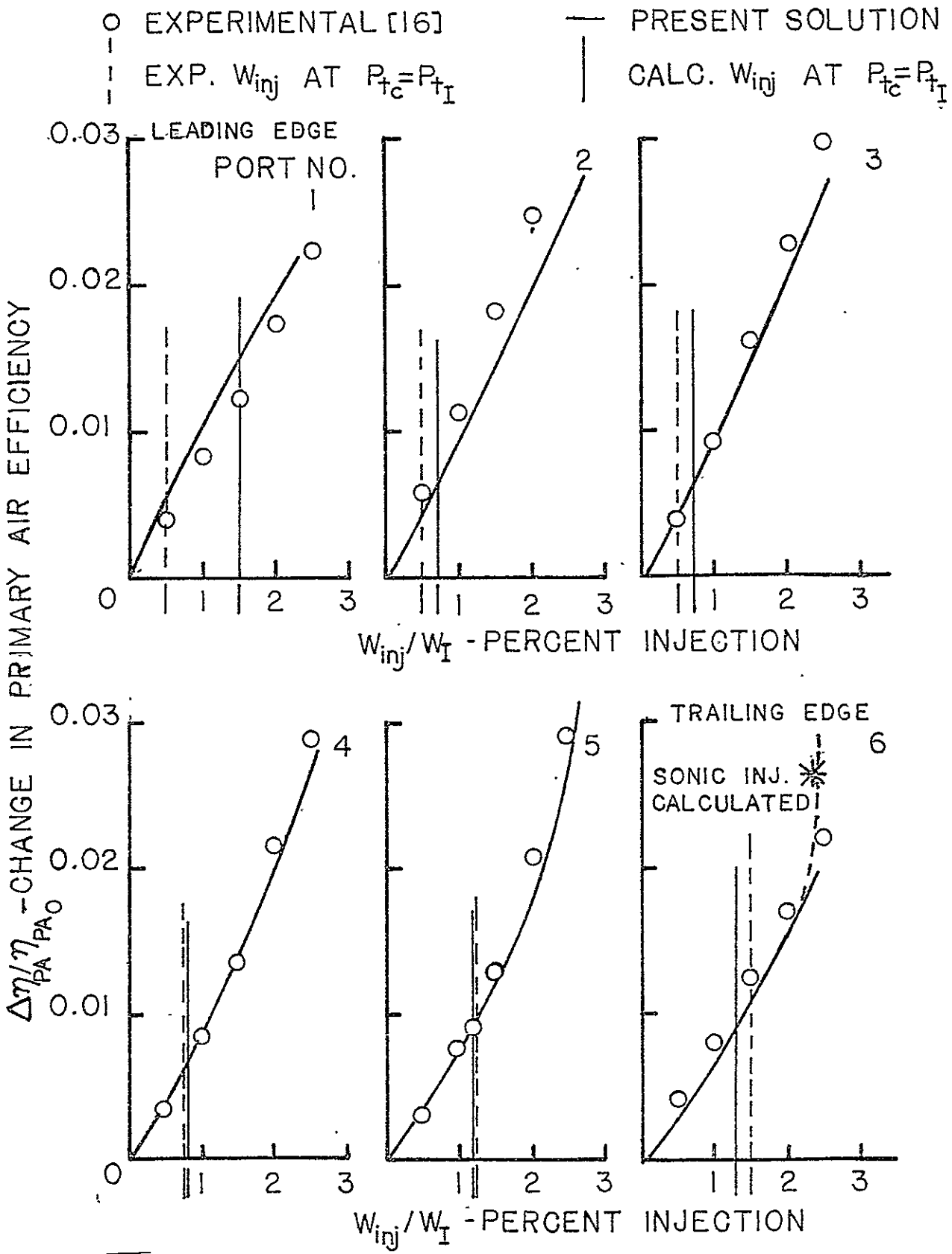

FIGURE 18. AERO-PERFORMANCE PRESSURE SIDE INJECTION

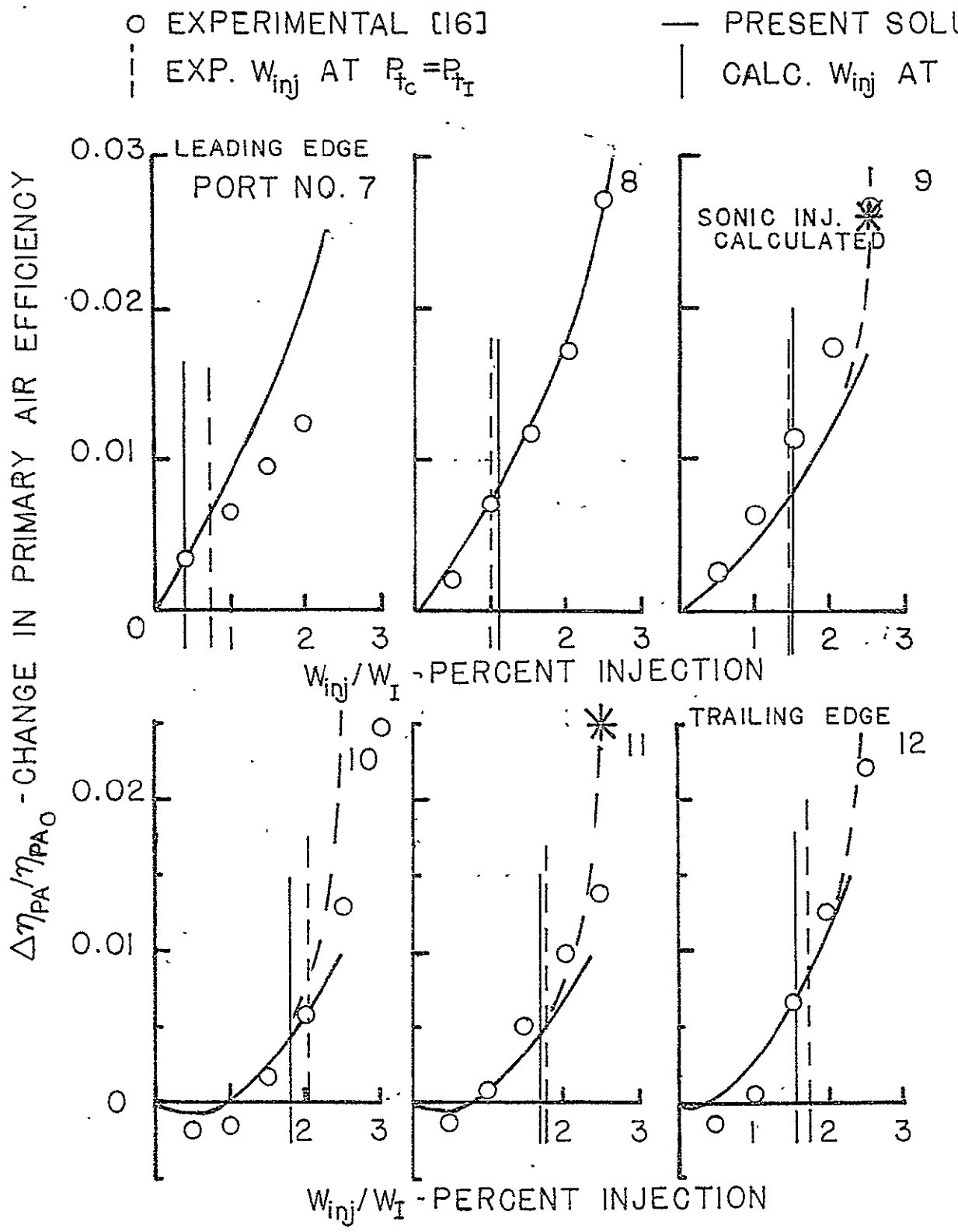

FIGURE 19. AERO-PERFORMANCE SUCTION SIDE INJECTION

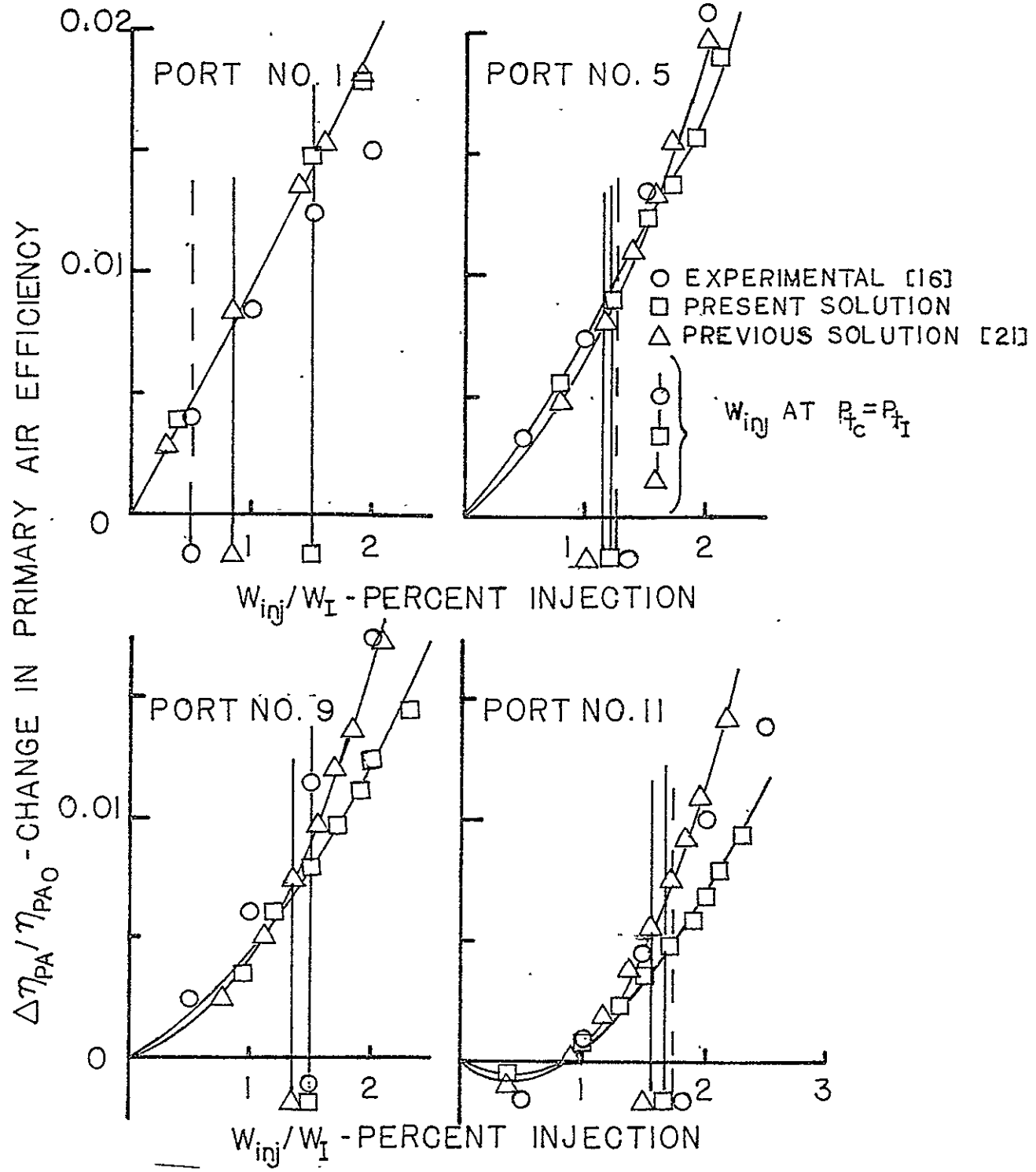

FIGURE 20. COMPARISON OF ANALYTICAL SOLUTIONS

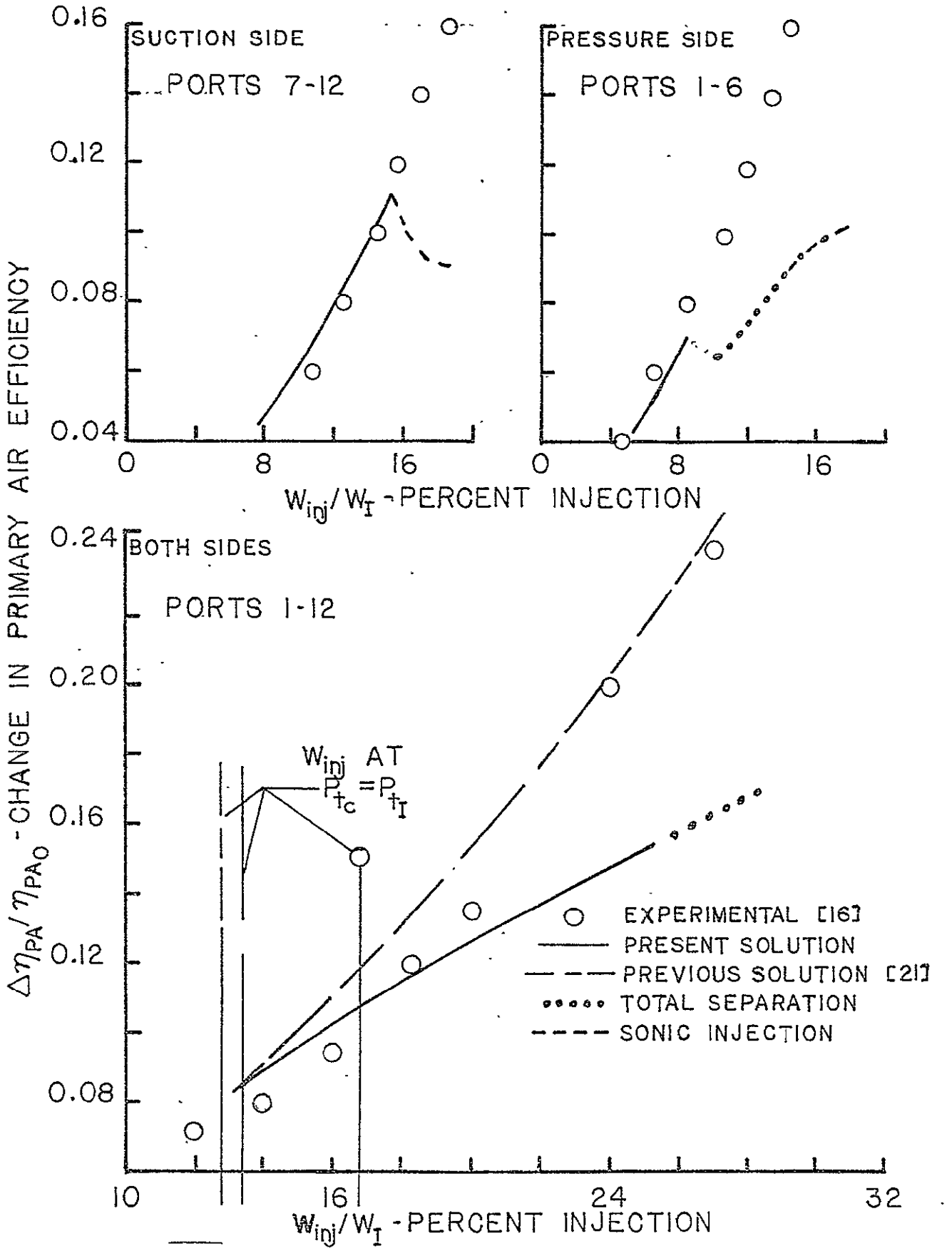

FIGURE 21.. MULTIPLE INJECTION ANALYSIS

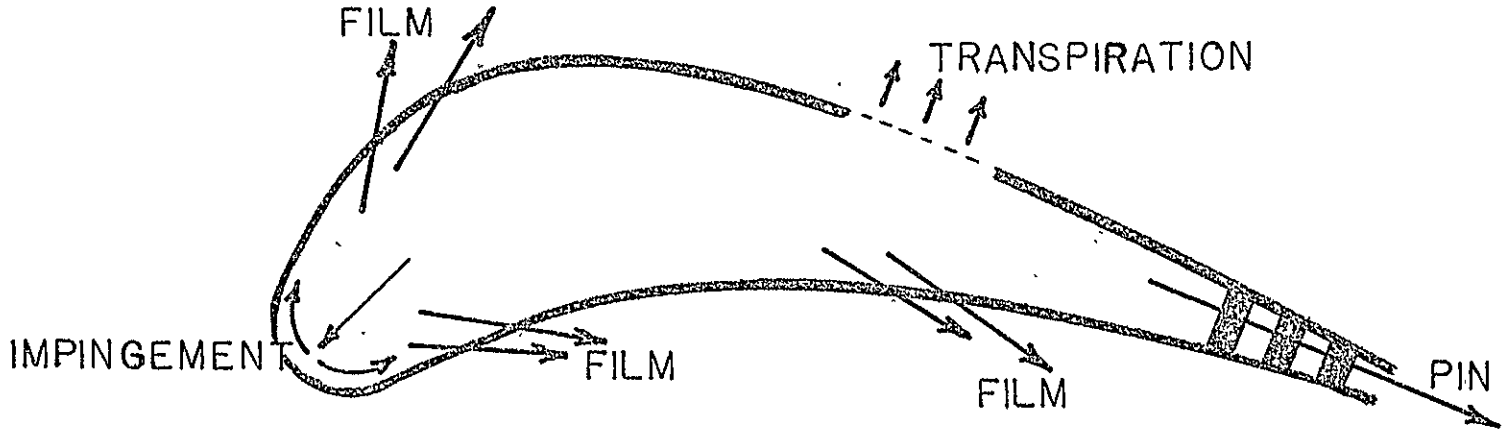

FIGURE 22. DESIGN TURBINE BLADE COOLING CONFIGURATION

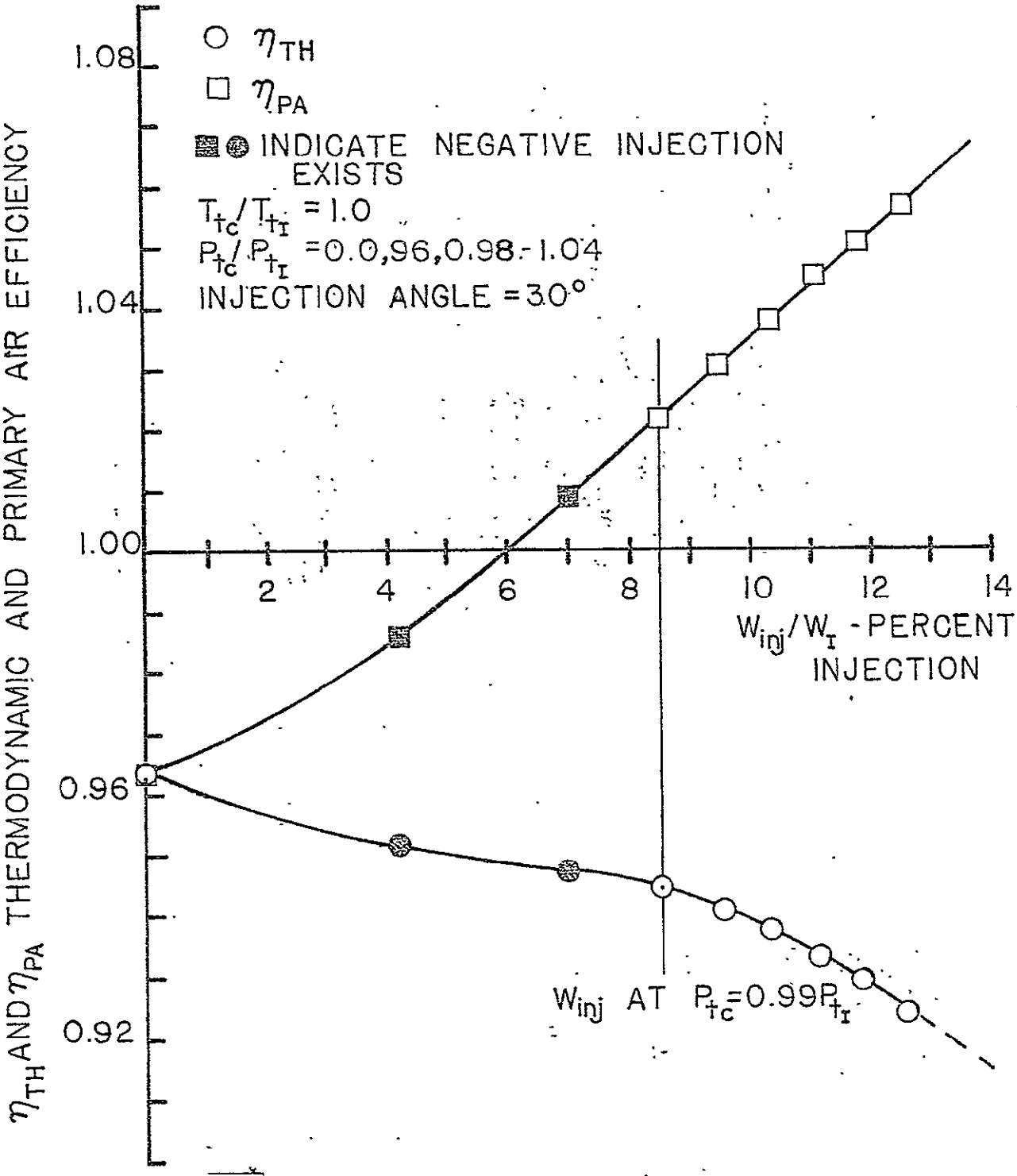

FIGURE 23. AERO-PERFORMANCE OF DESIGN CASCADE FOR VARIATIONS IN INJECTION MASS FLOW

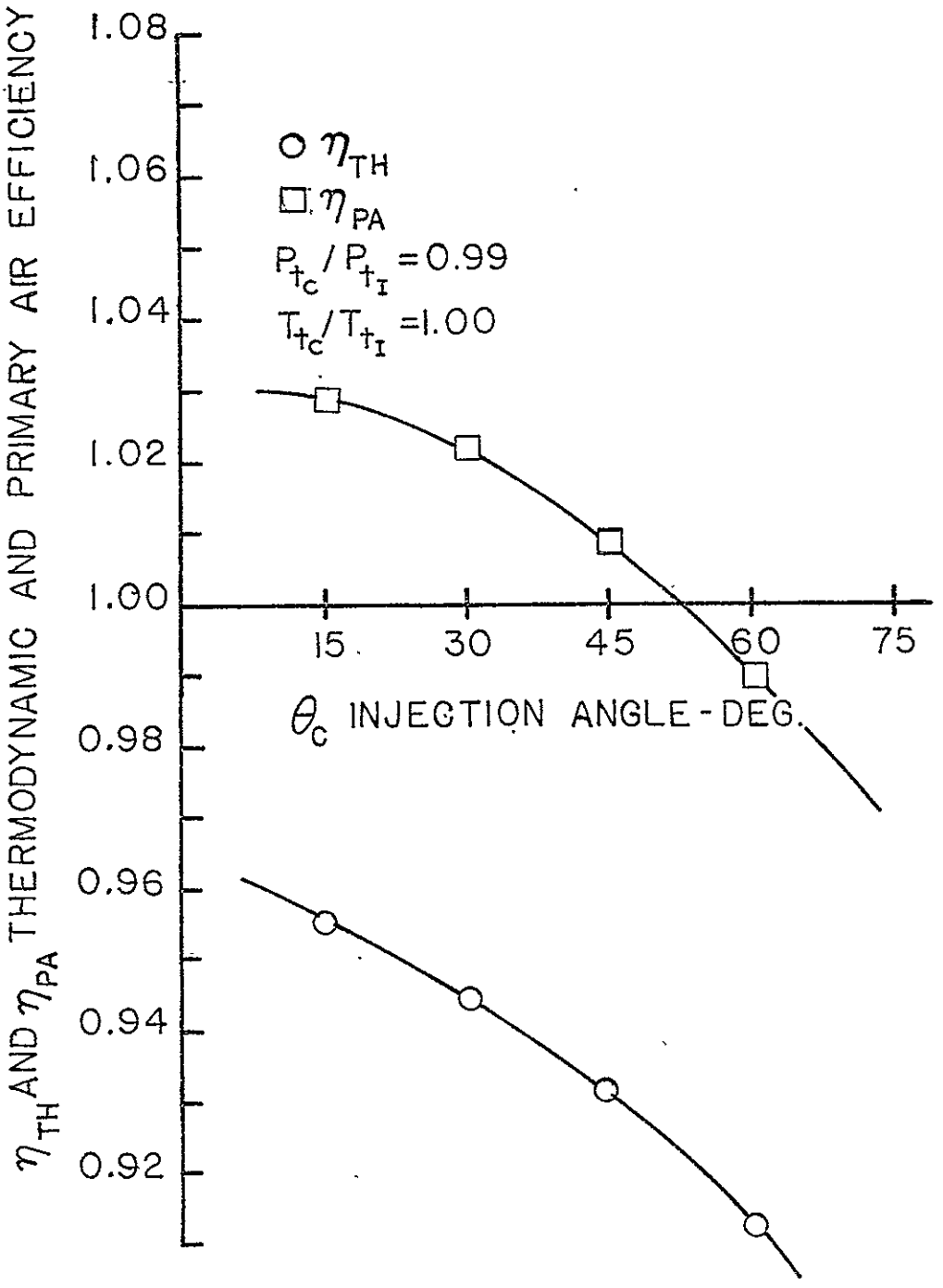

FIGURE 24. AERO-PERFORMANCE OF DESIGN CASCADE FOR VARIATIONS IN INJECTION ANGLE

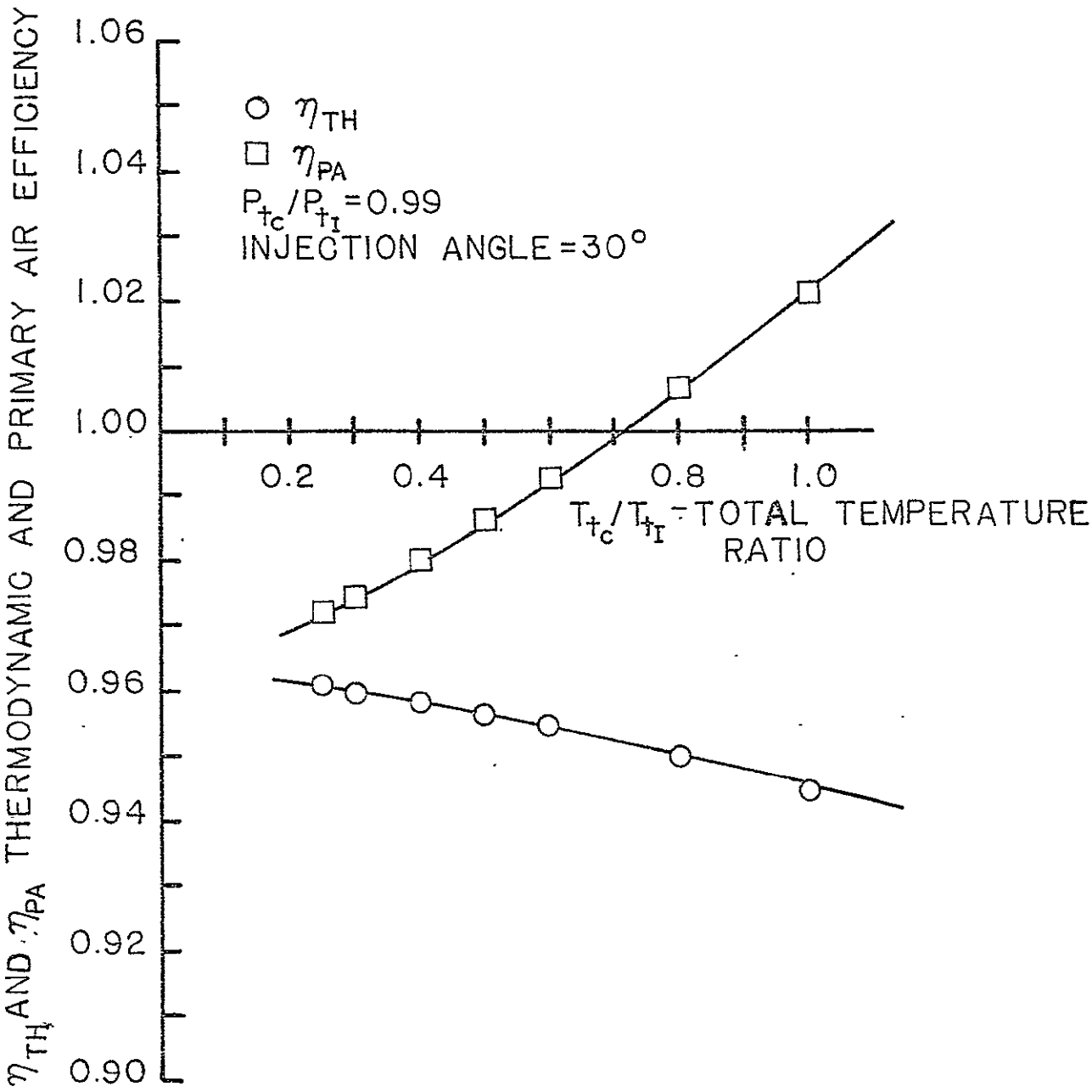

FIGURE 25. AERO-PERFORMANCE OF DESIGN CASCADE VARIATIONS IN INJECTION TOTAL TEMPERATURE

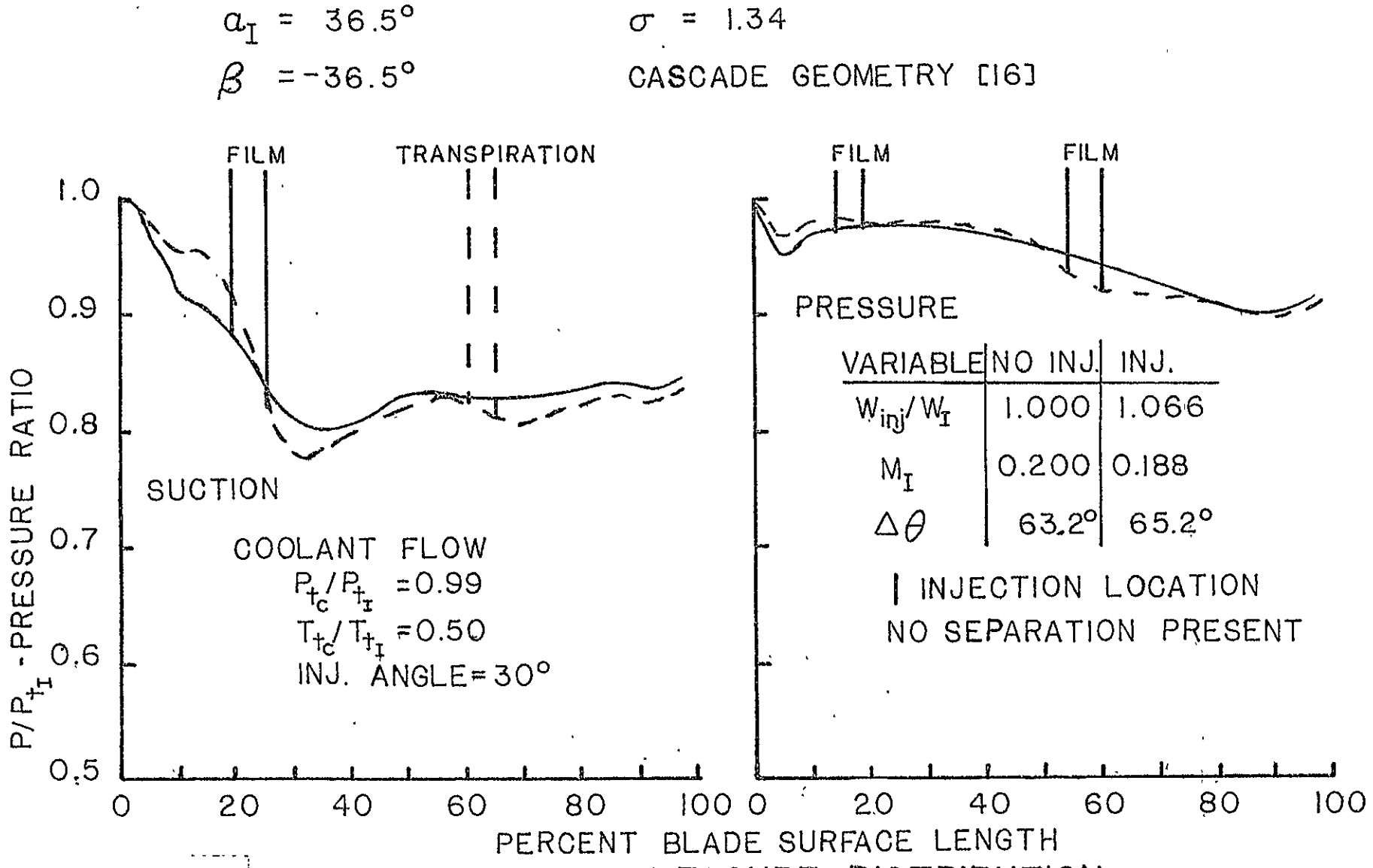

FIGURE 26, DESIGN CASCADE PRESSURE DISTRIBUTION

APPENDIX

MATRIX COEFFICIENTS

Singularity Influence Matrices

The problem is to calculate the velocity contribution that a distributed singularity has on a point. The singularity and the point have coordinate systems with varying orientations to a reference coordinate system. Resulting velocities are to be described in the point coordinate system. The general problem is shown in figure A-1. The reference coordinate system is x,y with points z, c_1 and c_2 locating the point coordinate system (p,q) and the singularity coordinate (η,ξ). The point and singularity coordinate systems are at an angle θ and ϕ with respect to the reference. All coordinate systems are complex. The prime notation indicates the coordinates of a point in the singularity or point of interest coordinate system. The surface singularity is distributed along the line segment of length ℓ which extends to $\pm \infty$ into and out of the plane. For a cascade, identical surface singularities occur at intervals of the cascade spacing, S, along a line parallel to the y axis. In this discussion the summed singularity of equation (31) in the analytical solution section is integrated to $\pm \infty$ in the out of plane direction and will be considered as a single singularity or velocity potential operating over the surface from c_1, c_2, into and out of the plane.

$$w = v_x - iv_y = 2\,\frac{k(\eta)\pi}{S}\,\coth\left(\frac{\pi(z'-\eta)}{S}\right) \tag{A1}$$

where

$$k(\eta) = s(\eta) + ig(\eta) \tag{A2}$$

Unit vectors aligned with the real axis of the point and singularity coordinate systems may be written in complex notation.

point unit vector = $e^{i\theta}$ (A3)

singularity unit vector = $e^{i\phi}$ (A4)

Constant Strength Singularity: For this case, the singularity strength is written as,

$$k(c) = k(\eta) = \text{constant}$$

The velocity effect in the reference coordinates is found as before in the analytical solution section

$$w = 2\frac{k\pi}{S}\int_{c_1}^{c_2} \coth\left(\frac{\pi(z-c)}{S}\right) dc \tag{A5}$$

$$w = -2k\,\bar{e}^{i\phi}\,\ell n\left\{\frac{\sinh(\pi(z-c_2)/S)}{\sinh(\pi(z-c_1)/S)}\right\} \tag{A6}$$

$$w(z") = v_p - iv_q = e^{i\theta}\,w(z)$$

$$w(z") = -2k\,\bar{e}^{i\theta}\bar{e}^{i\phi}\,\ell n\left\{\frac{\sinh(\pi(z-\eta_2)/S)}{\sinh(\pi(z-\eta_1)/S)}\right\} \tag{A7}$$

Equation (A7) applies for the general problem where the point of interest is removed from the singularity, but when the point lies on the singularity surface a Cauchy integral technique must be used to properly evaluate equations. When

$$z'(\eta,\xi) = z"(p,q) = 0+0i$$

then equation (A1) becomes

$$w(z) = 2\frac{k\pi}{S}\coth\left(-\frac{\pi c}{S}\right)$$

Following the same procedure as before the integral form is written as

$$w = 2\frac{k\pi}{S}e^{-i\phi}\int_{-\ell/2}^{+\ell/2}\coth\left(-\frac{\pi\eta}{S}\right)d\eta$$

The integration is carried out piecewise to isolate the singularity cross-over point at $\eta = 0$.

$$w = 2\frac{k\pi}{S}e^{-i\theta}\left[\int_{-\ell/2}^{-\delta}\coth\left(\frac{-\pi\eta}{S}\right)d\eta + \int_{-\delta}^{+\delta}\coth\left(\frac{-\pi\eta}{S}\right)d\eta\right.$$

$$\left. + \int\coth\left(\frac{-\pi\eta}{S}\right)d\eta\right]$$

where $\pm\delta$ define a small region around the origin.

Since the hyperbolic cotangent is an odd function along the real axis, and the distance $-\delta$ to $-\ell/2$ and $+\delta$ to $\ell/2$ are the same; the first and third integrals will exactly cancel.

$$w = 2\frac{k\pi}{S}e^{-i\phi}\int_{-\delta}^{+\delta}\coth\left(\frac{-\pi\eta}{S}\right)d\eta$$

In the neighborhood of the origin the coth (z) may be replaced by 1/z and by letting $u = -\pi\eta/S$, the integral is simplified.

$$w = -2k\,e^{-i\phi}\int_{-\delta}^{+\delta}\frac{1}{u}\,du$$

This integral can be evaluated by using an indented contour to arrive at the Cauchy Principle Value

$$w = -2k\, \bar{e}^{i\phi} \left[\int_{-\delta}^{-\rho} \frac{1}{u}\, du + \int_{-\rho}^{+\rho} \frac{1}{u}\, du + \int_{-\rho}^{+\delta} \frac{1}{u}\, du \right]$$

The first and third integrals cancel leaving

$$w = -2k\, \bar{e}^{i\phi} (-\pi i)$$

$$w(z") = e^{i\phi}\, w(z)$$

$$w(z") = 2\pi k i \tag{A8}$$

The influence matrix is formed by using the above formulas (A7-A8) to calculate the summed effects of all the body surface singularities on each of the central points on the body. The final form of the constant singularity strength influence matrix, A, is a n x n matrix with n being the number of singularities and control points. A single element of the matrix can be written as

$$a_{ij} = \left[2\pi i - \sum_{\substack{\alpha=1 \\ \alpha \neq i}}^{n} 2\, e^{i\theta i}\, \bar{e}^{i\phi\alpha} \ln \left\{ \frac{\sinh(\pi(z_i - c_{2\cdot})/S}{\sinh(\pi(z_i - c_{1\cdot})/S} \right\} \right] \tag{A9}$$

and is the coefficient of the strength k_i.

In the matrix form of equation (54) and (55) of the analytic solution section for calculating velocities and the source-sink strength distribution (s_k), the source-sink influence matrices are

$$[A_{s_{ij}}]_{nxn} = \text{Re}\,[A]_{nxn} \tag{A10}$$

$$[B_{s_{ij}}]_{nxn} = -\text{IM}\,[A]_{nxn} \tag{A11}$$

Linear Strength Singularity: The development of this coefficient matrix follows closely the development of the constant strength matrix. The only change being the form of strength function k in equation (A2).

$$k(\eta) = k(\eta_1) + \frac{k(\eta_2) - k(\eta_1)}{\eta_2 - \eta_1}(\eta - \eta_1)$$

$$= k(\eta_1) + \Delta(\eta - \eta_1) \tag{A12a}$$

$$k(\eta) = K(c_1) + \Delta(z - c_1) \tag{A12b}$$

Integrating the single surface singularity to find velocity contribution at a point gives

$$w(z) = 2\frac{\pi e^{-i\phi}}{S}\left[k(\eta_1)\int_{\eta_1}^{\eta_2}\coth\left(\frac{\pi(z'-\eta)}{S}\right)d\eta + \Delta\int_{\eta_1}^{\eta_2}(\eta-\eta_1)\coth\left(\frac{\pi(z'-\eta)}{S}\right)d\eta\right] \tag{A13}$$

Let

$$D = \int_{\eta_1}^{\eta_2}\coth\left(\frac{\pi(z'-\eta)}{S}\right)d\eta = -\frac{S}{\pi}\left\{\frac{\sinh[\pi(z-c_2)/S]}{\sinh[\pi(z-c_1)/S]}\right\} \tag{A14}$$

then

$$w(z) = -2e^{-i\phi}\left\{[k(z_1) - \Delta c_1]\,D - \frac{\Delta\pi}{S}\int_{\eta_1}^{\eta_2}\eta\coth\left(\frac{\pi(z'-\eta)}{S}\right)d\eta\right\} \tag{A15}$$

Direct evaluation of the remaining integral in equation (A15), results in an infinite series solution in which the coefficients of the terms are Bernoulli numbers. Rather than use this complicated solution form, an integral is formed in a piecewise manner using the defining complex series for the hyperbolic cotangent function

$$I = \frac{\pi}{S} \{ \int_{\eta_1}^{\eta_2} \eta \coth\left(\frac{\pi(z'-\eta)}{S}\right) d\eta \}$$

Expanding in series form

$$I = \frac{\pi}{S} \{ \int_{\eta_1}^{\eta_2} \eta \left(\frac{S}{\pi(z'-\eta)} + \frac{2\pi(z'-\eta)}{S}\right) \left[\frac{1}{\pi^2+\pi^2(z'-\eta)^2/S^2}\right.$$

$$\left. + \frac{1}{4\pi^2+\pi^2(z'-\eta)^2/S} + \frac{1}{9\pi^2+\pi^2(z'-\eta)^2/S^2} + \ldots\right] \}$$

$$I = \int_{\eta_1}^{\eta_2} \frac{\eta}{z'-\eta} d\eta + \sum_{\alpha=1}^{\infty} \int_{\eta_1}^{\eta_2} \frac{2\eta(z'-\eta)}{(z'-\eta)+(jS)^2} d\eta \qquad \text{(A16)}$$

Equation (A16) can now be integrated term by term to give a recursive relation for the integral

$$I = (c_1-c_2) - z \ln\left(\frac{z-c_2}{z-c_1}\right) + \sum_{\alpha=1}^{\infty} \{2(c_1-c_2)$$

$$+ 2jS\left[\tan^{-1}\left(\frac{z-c_1}{jS}\right) - \tan^{-1}\left(\frac{z-c_2}{jS}\right)\right]$$

$$- z \ln\left(\frac{(jS)^2+(z-c_2)^2}{(jS)^2+(z-c_1)^2}\right) \} \qquad \text{(A17)}$$

The index j corresponds to the number of bodies in the cascade row on either side of the point of interest being considered in

the velocity calculation. As the quantity, jS, becomes larger, the series terms contribute less to the velocity. In this solution the series evaluation was set up to include terms for the contributions of all cascade blades within distance of ten blade chords.

Combining all the terms in equations (A13), (A14) and (A17), the disturbance velocity becomes

$$w(z'') = -2e^{i\theta}\, e^{-i\phi}\left[\left\{k(c_1) - \frac{[k(c_2)-k(c_1)]}{(c_2-c_1)}\, c_1\right\} D - \frac{[k(c_2)-k(c_1)]}{(c_2-c_1)}\, I\right]$$

Gathering terms on the values of k

$$w(z'') = k(c_1)\left\{-2e^{i\theta}\, e^{-i\phi}\left[D + \frac{1}{(c_2-c_1)}\,(c_1 D + I)\right]\right\} + k(c_2)\left\{2\, e^{i\theta}\, e^{-i\phi}\left[\frac{c_1 D+I}{(c_2-c_1)}\right]\right\} \qquad \text{(A18)}$$

Again the effect of a surface singularity upon its own control point must be considered. The development is straightforward. It uses the evaluation of D from the constant strength analysis, and direct substitution into equation (A17) to find the value of I.

$$\text{at } z' = 0: \quad D = -\pi i$$

$$\text{at } z' = 0: \quad I = -\ell + \sum_{j=1}^{\infty} 2\left[-\ell + 2j\, \mathrm{Stan}^{-1}\left(\frac{\ell}{2jS}\right)\right]$$

Substituting into equation (A18) with $c_1 = -\ell/2$ and $c_2 = +\ell/2$ gives

$$w(z'') = k(-\ell/2)\left\{\pi i + \left[2 - 4 \sum_{j=1}^{\infty} \left(-1 + \frac{2jS}{\ell} \tan^{-1}\left(\frac{\ell}{2jS}\right)\right)\right] + k(\ell/2)\left\{-\pi i + \left[-2 + 4 \sum_{j=1}^{\infty} \left(-1 + \frac{2jS}{\ell} \tan^{-1}\left(\frac{\ell}{2jS}\right)\right)\right]\right\} \qquad \text{(A19)}$$

To formulate the linear matrix B, the coefficients for the singularity strengths at the end points of the approximating flat elements must be determined. The linear distribution required that the first and last elements have the same strength (i.e. $k_1 = k_{n+1}$). This causes several special cases to be added to the coefficient equations. For $j \neq m$, and $j \neq 1$, the coefficient of k_m is

$$b_{jm} = -2e^{i\theta_m} e^{-i\phi_j} \{D_j + \frac{c_j D_j + I_j}{c_{j+1} - c_j}\}$$

$$+ 2 e^{i\theta_m} e^{-i\phi_{j-1}} \{\frac{c_{j-1} D_{j-1} + I_{j-1}}{c_j - c_{j-1}}\} \quad \text{(A20)}$$

For $j \neq m$ and $j = 1$

$$b_{1m} = -2e^{i\theta_m} e^{-i\phi_1} \{D_1 + \frac{c_1 D_1 + I_1}{(c_2 - c_1)}\}$$

$$+ 2e^{i\theta_m} e^{-i\phi_n} \{\frac{c_n D_n + I_n}{c_{n+1} - c_1}\} \quad \text{(A21)}$$

For $j = m$ and $m \neq 1$

$$b_{mm} = \{\pi i + [2 - 4 \sum_{j=1}^{\infty} (-1 + \frac{2jS}{\ell_m} \tan^{-1}(\frac{\ell_m}{2jS}))]\}$$

$$+ 2e^{i\theta_m} e^{-i\phi_{m-1}} \{\frac{c_{m-1} D_{m-1} + I_{m-1}}{c_m - c_{m-1}}\} \quad \text{(A22)}$$

For $j = m+1$ and $m \neq n$

$$b_{m+1\ m} = -2e^{i\theta_m} e^{-i\phi_{m+1}} \{D_{m+1} + \frac{c_{m+1} D_{m+1} + I_{m+1}}{(c_{m+2} - c_{m+1})}\}$$

$$+ \{-\pi i + [-2 + 4 \sum_{j=1}^{\infty} (-1 + \frac{2jS}{\ell_m} \tan^{-1} (\frac{\ell_m}{2jS}))]\} \quad \text{(A23)}$$

For $j = m+1$ and $m = n$

$$b_{in} = -2e^{i\theta_n} e^{-i\phi_1} \{D_1 + \frac{c_1 D_1 + I_1}{(c_2 - c_1)}\}$$

$$+ \{-\pi i + [-2 + 4 \sum (-1 + \frac{2jS}{\ell_n} \tan^{-1}(\frac{\ell_n}{2jS}))]\} \qquad \text{(A24)}$$

For $j = m$ and $m = 1$

$$b_{11} = \{\pi i + [2 - 4 \sum_{j=1}^{\infty} (-1 + \frac{2jS}{\ell_1} \tan^{-1}(\frac{\ell_1}{2jS}))]\}$$

$$+ 2e^{i\theta_1} e^{-i\phi_n} \{\frac{c_n D_n + I_n}{c_{n+1} - c_n}\} \qquad \text{(A25)}$$

With equations (A20) through (A25), the coefficient matrix B may be formed for use in matrix form of (54) and (55) of the analytical solution section for the calculation of body velocities and determination of the vortex strength linear distribution (g_k).

$$[A_{v_{ij}}]_{nxn} = Re[iB]_{nxn} \qquad \text{(A26)}$$

$$[B_{v_{ij}}]_{nxn} = -Im[iB]_{nxn} \qquad \text{(A27)}$$

Minimization Equations Matrix Form

Recalling the general form of the equation system for finding the minimized singularity density, the formula needed for developing the details of the coefficient matrix may be written down.

$$Q = Q(g_1, g_2, \ldots g_3, \lambda_1, \lambda_2)$$

$$= \{[\Delta_{s_i}]_{1xn} [([\beta_i]_{nx1} + [C_{ik}]_{nxn} [g_k]_{nx1})^2]_{nx1}$$

$$+ [\Delta_{v_i}]_{1xn} [g_k^2]_{nx1} \} + \lambda_1 \{[B_{s_{TEi}}]_{1xn} [\beta_i]_{nx1}$$

$$+ [B_{s_{TEi}}]_{1xn} [C_{ik}]_{nxn} [g_k]_{nx1} + [B_{v_{TEj}}]_{1xn} [g_k]_{nx1}$$

$$- V_{onset} \sin(\theta_{TE} - \alpha)\} + \lambda_2 \{[C_{nk} - C_{1k}]_{1xn} [g_k]_{nx1}$$

$$- (\beta_1 - \beta_n)\} = 0$$

Taking the derivative of Q with respect to each of its independent variables and setting the result equal to zero, generates the minimization matrix equation. The derivative of Q with respect to g_j is in expanded form,

$$\frac{\partial Q}{\partial g_j} = 2\Delta_{s_1} C_{1j}(\beta_1 + C_{11}g_1 + C_{12}g_2 + \ldots C_{1j}g_j + \ldots C_{1n}g_n)$$

$$+ \ldots 2\Delta_{s_j} C_{jj}(\beta_j + C_{j1}g_1 + C_{j2}g_2 + \ldots C_{jj}g_j + \ldots C_{jn}g_n)$$

$$+ \ldots 2\Delta_{s_n} C_{nj}(\beta_n + C_{n1}g_1 + C_{n2}g_2 + \ldots C_{nj}g_j + \ldots C_{nn}g_n)$$

$$+ 2\Delta_{v_j} g_j + \lambda_1 (B_{s_{TE1}} C_{1j} + B_{s_{TE2}} C_{2j} + \ldots B_{s_{TEj}} C_{jj}$$

$$+ \ldots B_{s_{TEn}} C_{nj} + B_{v_{TEj}}) + \lambda_2 (C_{nj} - C_{1j}) = 0 \quad \text{(A28)}$$

The derivative with respect to λ_1 is

$$\frac{\partial Q}{\partial \lambda_1} = (B_{s_{TE1}} \beta_1 + B_{s_{TE2}} \beta_2 + \ldots B_{s_{TEj}} \beta_\alpha + \ldots B_{s_{TEn}} \beta_n)$$

$$+ B_{s_{TE1}} (C_{11} g_1 + C_{12} g_2 + \ldots + C_{1n} g_n)$$

$$+ \ldots B_{s_{TE}} (C_{j1} g_1 + C_{j2} g_2 + \ldots C_{jn} g_n)$$

$$+ \ldots B_{s_{TEn}} (C_{n1} g_1 + C_{n2} g_2 + \ldots C_{nn} g_n)$$

$$+ B_{v_{TE1}} g_1 + B_{v_{TE2}} g_2 + \ldots B_{v_{TEn}} g_n$$

$$- V_{onset} \sin(\theta_{TE} - \alpha) = 0 \qquad \text{(A29)}$$

The derivative with respect to λ_2 is

$$\frac{\partial Q}{\partial \lambda_2} = (C_{n1} - C_{11}) g_1 + (C_{n2} - C_{12}) g_2$$

$$+ \ldots (C_{nj} - C_{1j}) g_j + \ldots (C_{nn} - C_{nj}) g_n$$

$$- (\beta_1 - \beta_n) = 0 \qquad \text{(A30)}$$

After collecting multipliers of the independent variables and taking constant terms to the right hand side of the equations, the general coefficients are written. The coefficient of g_i in equation (A28) when $j \neq 1$ is

$$2(\Delta_{s_1} C_{1j} C_{1i} + \Delta_{s_2} C_{2j} C_{2i} + \ldots \Delta_{sj} C_{ij} C_{jj}$$

$$+ \ldots \Delta_{s_n} C_{nj} C_{ni})$$

and when $j = i$, coefficient of g_i becomes

$$2(\Delta_{s_1} C_{1j}^2 + \Delta_{s_2} C_{2j}^2 + \ldots \Delta_{sj} C_{jj}^2 + \ldots \Delta_{s_n} C_{nj}^2)$$

The coefficient of λ_1 in equation (A28) is

$$(B_{s_{TE1}} C_{1j} + B_{s_{TE2}} C_{2j} + \ldots B_{s_{TEn}} C_{nj} + B_{v_{TEj}})$$

and the coefficient of λ_2 is

$$(C_{nj} - C_{1j})$$

Finally, the equation constant is

$$-2(\Delta_{s_1} C_{1j} \beta_1 + \Delta_{s_2} C_{2j} \beta_2 + \ldots + \Delta_{s_n} C_{nj} \beta_n)$$

For equation (A29) the coefficient of g_i is

$$(B_{s_{TE1}} C_{1i} + B_{s_{TE2}} C_{2i} + \ldots + B_{s_{TEn}} C_{ni} + B_{v_{TEi}})$$

The coefficients of λ_1 and λ_2 are

$$(0)$$

and the equation constant is

$$[-(B_{s_{TE1}} \beta_1 + B_{s_{TE2}} \beta_2 + \ldots + B_{s_{TEn}} \beta_n) + V_{onset} \sin(\theta_{TE}-\alpha)]$$

For equation (A30), the coefficient of g_i is

$$(C_{ni} - C_{1i})$$

The coefficients of λ_1 and λ_2 are

$$(0)$$

and the equation constant is

$$(\beta_1 - \beta_n)$$

Using the coefficients and constants, a system of linear equations results which is solved for the minimum vortex strength density.

$$\begin{bmatrix} \frac{\partial Q}{\partial g_1} \sim \text{coefficients} \\ \frac{\partial Q}{\partial g_2} \sim \text{coefficients} \\ \vdots \\ \frac{\partial Q}{\partial g_n} \sim \text{coefficients} \\ \frac{\partial Q}{\partial \lambda_1} \sim \text{coefficients} \\ \frac{\partial Q}{\partial \lambda_2} \sim \text{coefficients} \end{bmatrix} \begin{bmatrix} g_1 \\ g_2 \\ \vdots \\ g_n \\ \lambda_1 \\ \lambda_2 \end{bmatrix} = \begin{bmatrix} \frac{\partial Q}{\partial g_1} \sim \text{constant} \\ \frac{\partial Q}{\partial g_2} \sim \text{constant} \\ \\ \frac{\partial Q}{\partial g_n} \sim \text{constant} \\ \frac{\partial Q}{\partial \lambda_1} \sim \text{constant} \\ \frac{\partial Q}{\partial \lambda_2} \sim \text{constant} \end{bmatrix} \tag{A31}$$

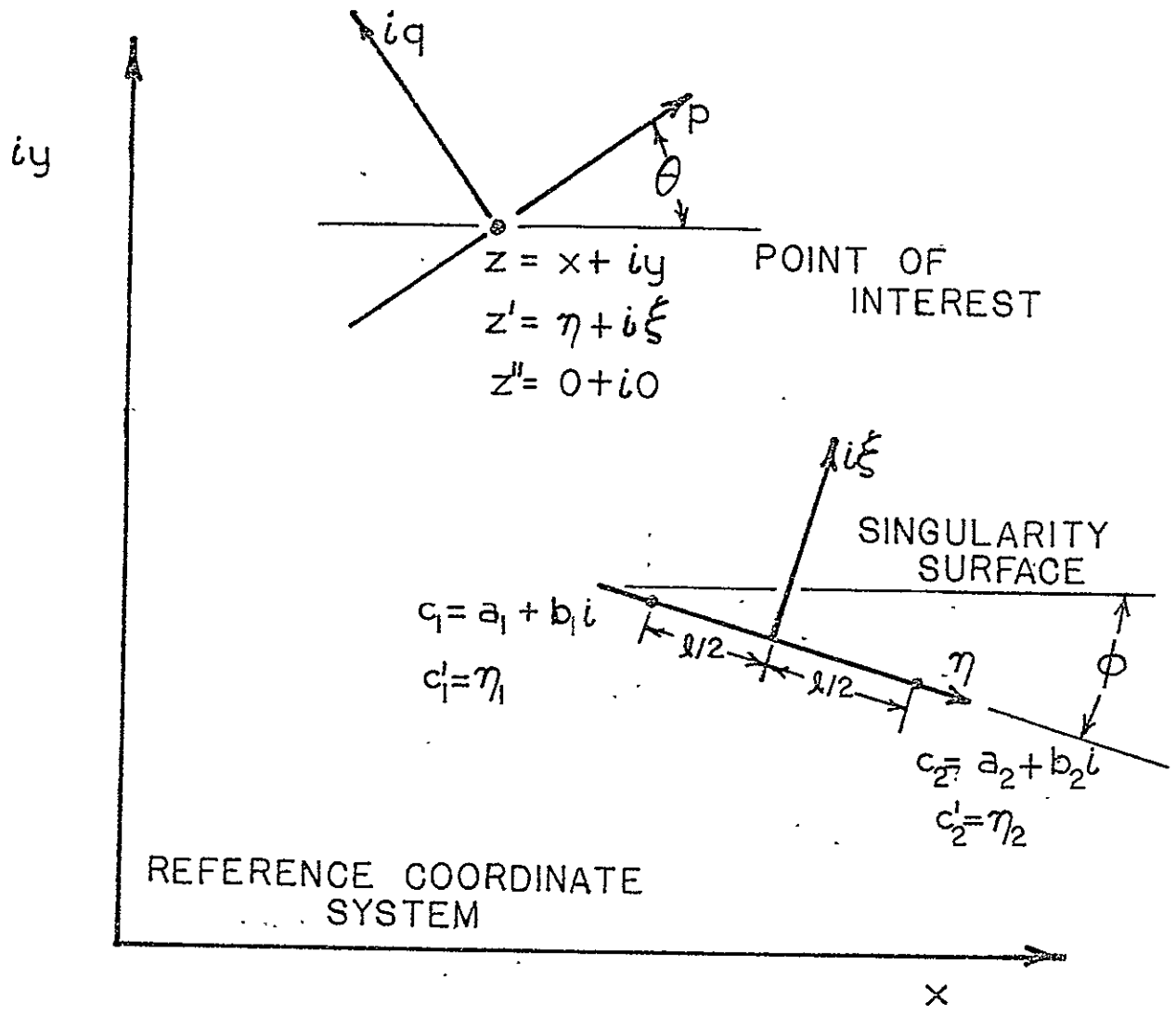

FIGURE A-I. SINGULARITY INFLUENCE PROBLEM